https://doi.org/10.1070/RCR4970

Electrodeposition of lanthanides from ionic liquids and deep eutectic solvents

Alexander V. Rudnev

A.N.Frumkin Institute of Physical Chemistry and Electrochemistry, Russian Academy of Sciences, Leninsky prosp. 31, korpus 4, 119071 Moscow, Russian Federation

Lanthanides belong to the most important raw materials and are highly demanded in high-tech industry. Low-temperature electrochemical deposition of lanthanides and lanthanide-based alloys for recycling and obtaining functional materials can provide a real alternative to the currently used high-temperature electrolysis of molten salts. The review summarizes the advancements in the field of electrodeposition of lanthanides from organic ionic systems, such as ionic liquids and deep eutectic solvents. The growing interest in these ionic systems is due to their excellent physicochemical properties, in particular non-volatility, thermal and electrochemical stability. The review also discusses further prospects and potential of the electrochemical approach for obtaining lanthanide-containing advanced materials.
The bibliography includes 219 references.

Contents

1. Introduction 1463
2. Deposition of lanthanides from halometallate ionic liquids 1466
3. Deposition from second-generation ionic liquids 1468
4. Electrochemical co-deposition of lanthanide-based alloys from ionic liquids 1474
5. Electrodeposition of lanthanides and lanthanide-based alloys from deep eutectic solvents 1476
6. Solubility and viscosity issues: challenges and prospects 1477
7. Conclusion 1479

1. Introduction

Lanthanides are rare-earth elements that are of great importance for a wide range of technologies and functional materials. Lanthanides are the key components of many modern products, such as catalytic systems, wind generators, solar panels, hard drives, mobile phones, electronic displays, LEDs, lasers, fibre optics, medical scanners, homing systems, night vision devices, *etc*.[1] Due to the unique configuration of unpaired f electrons and the complex structure of energy levels, lanthanides and their alloys exhibit unique optical, electrical and magnetic properties.[2] Recently, the European Commission included lanthanides in the list of 14 critical raw materials.[3,4] Furthermore, the primary extraction and processing of lanthanides based on traditional hydro- and pyrometallurgical processes have several drawbacks such as energy-intensive multistage operations, high operating temperatures, generation of toxic and radioactive waste due to the coextraction of thorium and uranium.[5–7] Given that the production and consumption of lanthanides are dominated by a single region (China),[5] this may lead to price volatility and problems with material availability. Therefore, reliable access to these materials and their effective use in the future as well as recycling are crucial for the sustainable development of lanthanide-based technologies. The advances in electrochemical methods for obtaining lanthanide-based coatings are of great interest for microelectronic industry, medicine, energy storage and conversion market, *etc*.[2] In this regard, the need to study and develop processes for electrodeposition of lanthanides involves both the creation of effective methods for extraction of these elements and preparation of novel functional materials with unique properties.

Lanthanides are very electropositive elements, much more electropositive than hydrogen, and possess very negative standard reduction potentials [*e.g.* $E^0(Nd^0/Nd^{3+}) = -2.323$ V *vs* SHE[8]]. The electrodeposition of lanthanides in aqueous solutions is practically unattainable because of a vigorous hydrogen evolution reaction (HER) at the cathode. Furthermore, the f elements react with water, forming hydroxides or oxides.[9,10] Thus, pure lanthanide metal films cannot be electrodeposited from aqueous solutions. To overcome the disadvantages of aqueous systems, lanthanides (Ln) and alloys can be produced both on a laboratory and industrial scale by molten salt electrolysis.[6,11] The electrochemical reduction of Ln(III) or Ln(II) from molten salts (*e.g.*, based on chlorides and/or fluorides of alkali metals) at rather high temperatures (typically >400 °C) was reported by many research groups to form high-purity crystalline films[12–16] of Ln(0) as well as Ln-based alloys.[17–22] However, molten salt electrolysis processes have crucial drawbacks: a highly corrosive environment and high energy consumption. Electrochemical deposition of lanthanides at room temperature was attempted from organic solvents: such as dimethylformamide (DMFA), formamide, dimethyl sulfoxide, acetonitrile, ethanol.[23–28] However, flammability and volatility of organic solvents are dangerous and harmful to the health

A.V.Rudnev. PhD in Chemistry, Leading Researcher at the IPCE RAS. Telephone: +7(495)955–4456, e-mail: rudnev@phyche.ac.ru
Current research interests of the authors: electrocatalysis, electrodeposition of metals and alloys, electrochemistry of single crystals, ionic liquids and deep eutectic solvents, adsorption processes, surface modification by organic molecules and inorganic nanoobjects, molecular electronics, scanning probe microscopy.

Received 15 June 2020

© 2020 Uspekhi Khimii, ZIOC RAS, Russian Academy of Sciences and IOP Publishing Limited

and the environment, which is a key barrier for industrial application of such systems.[29]

Ionic liquids (ILs) consisting of organic ions are attracting increasing attention as new electrochemical media and as a potential replacement for high-temperature salt melts and organic solvents in electrodeposition processes both on a laboratory and industrial scale. This interest is due to unique physicochemical properties of ILs: non-volatility, non-flammability, heat resistance, intrinsic ionic conductivity, electrochemical stability, good solubility of metal salts, the ability to tune properties by combining and modifying organic ions.[30–32] Of particular interest are second-generation ILs that consist of asymmetric organic cations, such as dialkylimidazolium, dialkylpyrrolidinium, tetraalkylammonium, *etc.*, and anions, for example, $[PF_6]^-$, $[OTf]^-$, $[TFSI]^-$, $[DCA]^-$ (Fig. 1 and Table 1). Compared to haloaluminate (first-generation) ILs, the ILs of the second generation are stable in air and in the presence of water and have a wider electrochemical window (typically >4.0 V).[31,33] The possibility of electrodeposition from IL-based solutions was demonstrated for various metals and semiconductors from the first to sixteenth groups of the periodic table.[33–38]

Recently, a new class of ionic systems, the so-called deep eutectic solvents (DESs), has gained attention as a possible medium for electrochemical deposition. Deep eutectic solvents (DESs) are systems formed from a eutectic mixture of Lewis or Brønsted acids and bases and can be classified according to the nature of the complexing agent used.[39] Type III DESs are mixtures of quaternary ammonium salts as hydrogen bond acceptors (HBAs) and other components as hydrogen bond donors (HBDs), such as amides, alcohols and acids.[40] The melting point of such eutectic mixtures can dramatically decrease due to the formation of hydrogen bonds (or other weak interactions): for example, choline chloride – urea (1 : 2) DES has a melting point of 285 K, while the melting point of urea and decomposition temperature of choline chloride are 406 K and 575 K, respectively. Type IV eutectic mixtures are mixtures of metal salts (*e.g.*, chloride or nitrate) and HBD. Such mixtures are of particular interest because they form cationic metal complexes, providing a high concentration of metal ions at the negatively charged electrode surface during electrodeposition.[41]

Deep eutectic solvents (DESs) have properties similar to those of ILs, including good conductivity (although not all DESs are conductive).[39] At the same time, they have additional advantages over ILs, such as the ease and low cost of synthesis. Moreover, despite their non-volatility (eliminating the safety and environmental problems often associated with volatile organic solvents), ILs typically exhibit low biodegradability and significant toxicity towards organisms from different trophic levels as pointed out in literature.[32,42] On the contrary, some DESs are characterized by non-toxicity and biodegradability, although the 'greenness' of a DES is dependent on the constituent materials:[43] DESs containing metal salts exhibit significantly higher toxicity than type III DESs (organic salts and HBDs).[44,45]

This review presents a comprehensive overview of the studies of electrochemical deposition of lanthanides and lanthanide-based alloys from ILs and DESs. The main results on lanthanide salt solubility in the organic ionic systems, their solvation structure, electrochemical behaviour, nucleation and growth of lanthanide-based deposits as well as their microscopic and spectroscopic characterisation are reviewed in the following sections. Finally, the challenges and prospects of the electrochemical approach to the production of lanthanide-based coatings are discussed. The structures of common IL cations and anions are presented in Fig. 1, while the names and abbreviations can be found in Table 1. Tables 1 and 2 also provide literature data on dynamic viscosity of ILs and DESs and diffusion coefficients of lanthanide ions in different ionic systems, respectively.

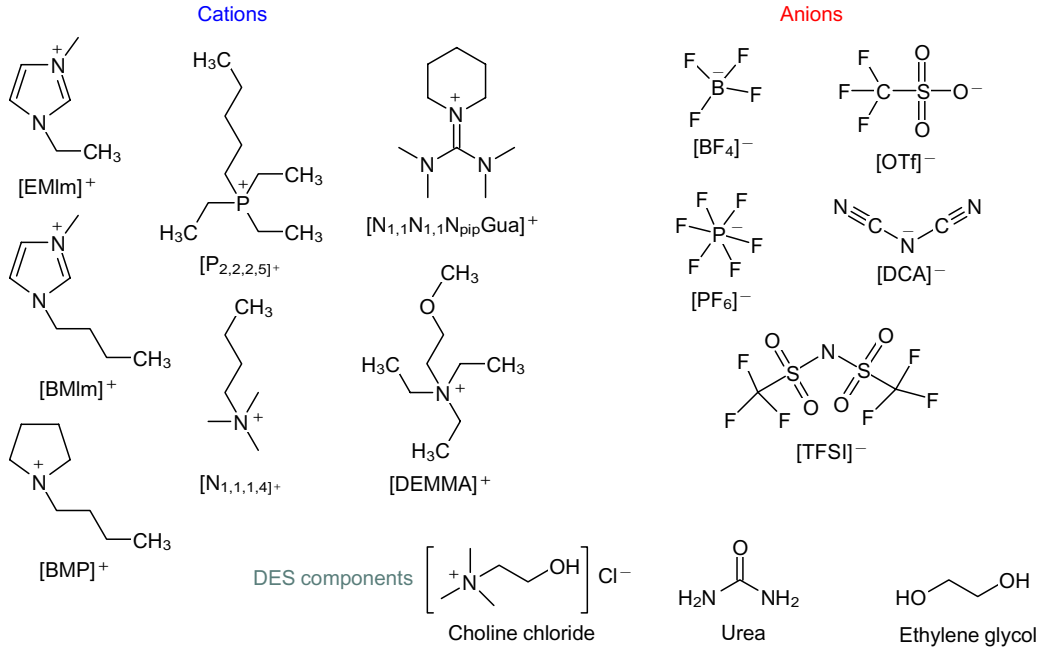


Figure 1. Cations and anions employed as components in non-haloaluminate ILs and DES components.

Table 1. Typical ILs and DESs and their dynamic viscosity.

Name	Notation	η /mPa s	T/K	Ref.
First-generation **ILs**				
1-Ethyl-3-methylimidazolium tetrachloroaluminate	[EMIm][$AlCl_4$]	21	293	46
1-Butyl-3-methylimidazolium tetrachloroaluminate	[BMIm][$AlCl_4$]	34	293	47
1-Ethyl-3-methylimidazolium heptachlorodialuminate	[EMIm][Al_2Cl_7]	16	293	46
Second-generation **ILs**				
1-Ethyl-3-methylimidazolium tetrafluoroborate	[EMIm][BF_4]	44	293	48
		36	298	48
1-Butyl-3-methylimidazolium tetrafluoroborate	[BMIm][BF_4]	141	293	48 – 50
		108	299	48 – 50
1-Butyl-3-methylimidazolium hexafluorophosphate	[BMIm][PF_6]	394	293	50
1-Butyl-3-methylimidazolium trifluoromethanesulfonate	[BMIm][OTf]	112	293	51
		129	293	50
1-Butyl-1-methylpyrrolidinium trifluoromethanesulfonate	[BMP][OTf]	158	293	52
1-Ethyl-3-methylimidazolium bis(trifluoromethane)sulfonimide	[EMIm][TFSI]	40	293	53
		39	293	48, 51
		32	298	48
1-Butyl-3-methylimidazolium bis(trifluoromethane)sulfonimide	[BMIm][TFSI]	50	293	54
		63	293	51, 53
1-Butyl-1-methylpyrrolidinium bis(trifluoromethane)sulfonimide	[BMP][TFSI]	96	293	51
		77	298	54
		84	298	55
1-Octyl-1-methylpyrrolidinium bis(trifluoromethane)sulfonimide	[OMP][TFSI]	130	298	56
Butyltrimethylammonium bis(trifluoromethane)sulfonimide	[$N_{4,1,1,1}$][TFSI]	138	293	55
		116	298	57
Triethyl(pentyl)phosphonium bis(trifluoromethane)sulfonimide	[$P_{2,2,2,5}$][TFSI]	88	298	58
Trihexyl(tetradecyl)phosphonium bis(trifluoromethane)sulfonimide	[$P_{6,6,6,14}$][TFSI]	454	293	59
N,*N*-Diethyl-*N*-methyl-*N*-(2-methoxyethyl)ammonium bis(trifluoromethane)sulfonimide	[DEMMA][TFSI]	120	298	60
N,*N*,*N*′,*N*′-Tetramethyl-*N*″,*N*″-pentamethyleneguanidinium bis(trifluoromethane)sulfonimide	[$N_{1,1}N_{1,1}N_{pip}$Gua][TFSI]	108	298	61
1-Ethyl-3-methylimidazolium dicyanamide	[EMIm][DCA]	17	293	48
		14	298	48
		21	293	62
1-Butyl-3-methylimidazolium dicyanamide	[BMIm][DCA]	37	293	50
		29	298	63
1-Butyl-1-methylpyrrolidinium dicyanamide	[BMP][DCA]	50	293	62
Ethyltributylammonium dicyanamide	[$N_{4,4,4,2}$][DCA]	340	298	63
1-Butyl-3-methylimidazolium tricyanomethanide	[BMIm][TCM]	34	293	64
1-Butyl-3-methylimidazolium tetracyanoborate	[BMIm][TCB]	41	293	64
DESs				
Choline chloride – urea (1 : 2)	reline	750	298	65
Choline chloride – ethylene glycol (1 : 2)	ethaline	37	298	65
$Ce(NO_3)_3 \cdot 6\,H_2O$ – urea (1 : 3.5)	CeDES	168	298	66
$Pr(NO_3)_3 \cdot 6\,H_2O$ – urea (1 : 3.5)	PrDES	181	298	66
$Nd(NO_3)_3 \cdot 6\,H_2O$ – urea (1 : 3.5)	NdDES	168	298	66

The following abbreviations and designations are used in the review:

CA — chronoamperometry,
CP — chronopotentiometry,
CV — cyclic voltammetry,
DES — deep eutectic solvent,
DHOA — *N*,*N*-dihexyl octanamide,
EDX — energy dispersive X-ray,
EDXRF — energy dispersive X-ray fluorescence,
EG — ethylene glycol
IL — ionic liquid,
GC — glassy carbon,
HBA — hydrogen bond acceptor,
HBD — hydrogen bond donor,
HER — hydrogen evolution reaction,
MS — molecular solvent,
NLIL — neutral-ligand ionic liquid,
RDE — rotating disc electrode,
SD — semi-differential analysis,
SEM — scanning electron microscopy,
SI — semi-integral analysis,
SPM — scanning probe microscopy,
TBP — tributyl phosphate,
TEM — transmission electron microscopy,
TM — transition metal,
TMP — trimethyl phosphate,
TODGA — *N*,*N*,*N*′,*N*′-tetraoctyl diglycolamide,
XPS — X-ray photoelectron spectroscopy,
XRD — X-ray diffraction.

2. Deposition of lanthanides from halometallate ionic liquids

Chronologically the electrochemical behaviour of lanthanides from ILs was first studied in haloaluminate ILs. However, the reports on the electrodeposition of lanthanides from haloaluminate ILs are rather scarce. Back in early 1980s, the electrochemistry of lanthanides was investigated in room-temperature [BPy][Cl] – $AlCl_3$ melts ([BPy][Cl] is 1-n-butylpyridinium chloride).[67, 68] The reversibility of the redox transformations Sm(III) ⇆ Sm(II), Yb(III) ⇆ Yb(II), Eu(III) ⇆ Eu(II), Tm(III) ⇆ Tm(II) was demonstrated by cyclic voltammetry (CV) in acidic [BPy][Cl] – $AlCl_3$ melts (with the molar fraction of $AlCl_3$ x_{AlCl3} ranged from 0.57 to 0.66) at 313 K. Relatively high diffusion coefficients were estimated for respective trivalent lanthanides (Table 2). Moreover, very different half-wave potentials ($E_{1/2}$) were obtained for the following Ln(III)/Ln(II) pairs: 0.020 V (Tm), 0.660 V (Sm), 1.230 V (Yb) and 1.855 V (Eu) *vs* an Al reference electrode,[67, 68] indicating that electrochemical properties vary significantly for different lanthanides. Such difference was rationalized in the terms of the refined electron spin pairing energy theory developed by Jørgensen [69] and Nugent *et al.*[70] According to these studies, $E_{1/2}$ of Ln(III)/Ln(II) pairs is determined by the number of *f* electrons (*q*). Similar trends of $E_{1/2}$ *vs q* for

Table 2. Diffusion coefficients (*D*) of lanthanides in different ILs and DESs, the respective lanthanide salts, their concentrations, measurement temperature and methods for *D* estimation. *D* values were mainly estimated using the response analysis of the Ln(III) → Ln(II) electrochemical reactions. Additionally, selected data for Co(II) and Fe(II) in ILs and DESs as well as for Eu(III) in an aqueous solution are given for comparison.

Ln ion	Salt and concentration	Ionic melt, IL, DES	*T*/K	$D \times 10^{12}$ /m^2 s^{-1}	Method [a]	Ref.
La(III)	0.08 M $LaCl_3$	[BMIm][DCA]	333	1.21×10^{-2}	CV, CA	133
Yb(III)	0.0033 mol kg^{-1} $YbCl_3$	[BPy][Cl] – $AlCl_3$ (x_{AlCl3} = 0.65)	313	31.5	CV, CA	67
Yb(III)	0.0114 M $YbCl_3$	[EMIm][Cl] – $AlCl_3$ (x_{AlCl3} = 0.667)	300	56.0	RDE, CV, CA	78
Yb(III)	0.0114 M $YbCl_3$	[EMIm][Cl] – $AlCl_3$ (x_{AlCl3} = 0.490)	300	35.4	RDE, CV, CA	78
Yb(III)	0.0114 M $YbCl_3$	[EMIm][Cl] – $AlCl_3$ (x_{AlCl3} = 0.444)	300	19.9	RDE, CV, CA	78
Yb(III)	0.1 M Yb(TFSI)$_3$	[BMP][TFSI]	298	3.6	CA	82
Yb(III)	0.030 M by anodic dissolution	[BMP][TFSI]	323	12.4	RDE	81
Yb(II)	0.0065 M by anodic dissolution	[BMP][TFSI]	323	11.4	RDE	81
Ce(III) [b]	~0.015 M $CeCl_3$	[EMIm][Cl] – $AlCl_3$ (x_{AlCl3} = 0.51)	313	37	CV	147
Ce(III)	0.05 M $EuCl_3$	[BMIm][Cl]	343	1.79	CV	131
Eu(III)	0.058 M $EuCl_3$	[EMIm][Cl]	363	44	CV, CA, SI, RDE	132
Eu(III)	0.040 M $EuCl_3$	[BMIm][Cl]	343	4.5	CV, CA, SI, RDE	132
Eu(III)	0.05 M $EuCl_3$	[BMIm][Cl]	343	4.87	CV	131
Eu(III)	0.05 M $EuBr_3$	[BMIm][Br]	293	0.97	CV	148
Eu(III)	0.01 M Eu(TFSI)$_3$	[$P_{2,2,2,5}$][TFSI]	298	2.6	CA	149
Eu(III)	0.01 M Eu(TFSI)$_3$	[$N_{2,2,2,5}$][TFSI]	298	1.2	CA	149
Eu(III)	0.1 M Eu(TFSI)$_3$	[BMP][TFSI]	298	3.1	CA	82
Eu(III)	0.05 M Eu(TFSI)$_3$(H_2O)$_3$	[BMP][TFSI]	298	2.94	CV, CP, CA	85
Eu(III)	0.030 M by anodic dissolution	[BMP][TFSI]	323	11.9	RDE	81
Eu(II)	0.032 M by anodic dissolution	[BMP][TFSI]	323	11.6	RDE	81
Eu(III)	0.05 M Eu(TFSI)$_3$	[BMP][TFSI]	298	4.2	CA	115
Eu(II)	0.05 M by reduction of Eu(III)	[BMP][TFSI]	298	3.9	CA	115
Eu(III)	0.1 M Eu(TFSI)$_3$	[EMIm][TFSI]	298	7.8	CA	82
Eu(III)	0.05 M $EuCl_3$	[BMIm][DCA]	303	26.5	CV	63
Eu(III)	0.05 M $EuCl_3$	[BMMIm][DCA]	303	6.52	CV	63
Eu(III)	0.05 M $EuCl_3$	[$N_{4,4,4,2}$][DCA]	303	7.44×10^{-2}	CV	63
Eu(III)	0.05 M $EuCl_3$	[$N_{8,4,4,4}$][DCA]	303	6.15×10^{-2}	CV	63
Eu(III)	0.01 M Eu(ClO_4)$_3$	[BMIm][TFSI], dehydrated	298	2.3	CV	60
Eu(III)	0.01 M Eu(ClO_4)$_3$	[BMIm][TFSI], water-saturated	298	8.9	CV	60
Eu(III)	0.01 M Eu(ClO_4)$_3$	[DEMMA][TFSI], dehydrated	298	1.6	CV	60
Eu(III)	0.01 M Eu(ClO_4)$_3$	[DEMMA][TFSI], water-saturated	298	4.6	CV	60
Eu(III)	0.09 M Eu(TFSI)$_3$	DHOA	353	2.3	CV	144
Sm(III)	10^{-3} mol kg^{-1} $SmCl_3$	[BPy][Cl] – $AlCl_3$ (x_{AlCl3} = 0.65)	313	30.0	CV, CA	67
Sm(III)	0.05 M $EuCl_3$	[BMIm][Cl]	343	3.17	CV	131
Sm(III)	0.01 M Sm(TFSI)$_3$	[$P_{2,2,2,5}$][TFSI]	298	2.8	CA	149
Sm(III)	0.01 M Sm(TFSI)$_3$	[$N_{2,2,2,5}$][TFSI]	298	1.3	CA	149
Sm(III)	0.1 M Sm(TFSI)$_3$	[BMP][TFSI]	298	3.1	CA	82
Sm(III)	0.032 M by anodic dissolution	[BMP][TFSI]	323	11.5	RDE	81
Sm(III)	0.041 M Sm(TFSI)$_3$(H_2O)$_3$	[$N_{1,1,1,4}$][TFSI]	298	4.7	CV	100
Nd(III)	0.5 M Nd(TFSI)$_3$	[$P_{2,2,2,5}$][TFSI]	373	0.6	CP	107
Nd(III)	0.5 M Nd(TFSI)$_3$	[DEMMA][TFSI]	353	0.15	SD, SI	106
Nd(III)	0.17 M Nd(TFSI)$_3$	TMP	298	4.25×10^{-2}	CV	143
Nd(III)	0.105 M Nd(TFSI)$_3$	DHOA	323	1.54	CV	144
Nd(III)	0.105 M Nd(TFSI)$_3$	DHOA	353	3.76	CV	144
Dy(III)	0.147 M Dy(TFSI)$_3$	[BMP][TFSI]	298	2.0	CV	86
Dy(III)	0.075 M Dy(TFSI)$_3$	[[$P_{2,2,2,5}$][TFSI]	298	2.0	SI	104
Dy(III)	0.1 M Dy(TFSI)$_3$	[[$P_{2,2,2,5}$][TFSI]	318	1.1	SI	105
Dy(III)	0.5 M Dy(TFSI)$_3$	[[$P_{2,2,2,5}$][TFSI]	333	4×10^{-2}	SI	104

Table 2 (continued).

Ln ion	Salt and concentration	Ionic melt, IL, DES	T/K	$D \times 10^{12}$/m^2 s^{-1}	Method [a]	Ref.
Dy(III)	0.154 M $Dy(TFSI)_3$	TMP	298	$2.2\ 10^{-2}$	CV	143
Dy(III)	0.094 M $Dy(TFSI)_3$	DHOA	323	0.8	CV	144
Dy(III)	0.094 M $Dy(TFSI)_3$	DHOA	353	1.9	CV	144
Gd(III)	0.22 M $Gd(TFSI)_3$	TMP	298	1.04×10^{-2}	CV	143
Pr(III)	0.173 M $Gd(TFSI)_3$	TMP	298	1.14×10^{-1}	CV	143
Fe(II)	0.1 M $Fe(TFSI)_2$	[BMP][TFSI]	298	9.7	CA	110
Co(II)	0.1 M $Co(TFSI)_2$	[BMP][TFSI]	301	10	CP	111
Co(II)	0.038 M $CoCl_2$	Reline	373	19.8	CA	150
Co(II)	0.05 M $CoCl_2$	Glyceline [c]	343	27.2	CA	151
Eu(III)	0.01 M $Eu(ClO_4)_3$	Aqueous solution	298	1.62×10^3	CV	60

Note. CV is cyclic voltammetry, CA is chronoamperometry, SI is semi-integral analysis, SD is semi-differential analysis, RDE is rotating disc electrode, CP is chronopotentiometry. [a] If several methods were used, an average value is given in the table; [b] $D_{Ce(III)}$ was estimated from the CV peak corresponding to Ce(III) oxidation to Ce(IV) on a GC electrode; [c] glyceline is choline chloride/glycerol (1 : 2 molar ratio).

Ln(III)/Ln(II) (but affected by the solvating power of the solvent [68]) were also observed in aqueous solutions, different organic solvents and high-temperature ionic melts.[70 – 72]

Tsuda *et al.*[73, 74] investigated the deposition of LaAl alloys from a saturated $LaCl_3$ solution in an acidic [EMIm][Cl] – $AlCl_3$ melt with $x_{AlCl3} = 0.667$. This mole fraction leads to the formation of $[EMIm][Al_2Cl_7]$ IL. Based on Raman data, the dissolution of $LaCl_3$ in $[EMIm][Al_2Cl_7]$ occurs by the following equation:

$$3\,[Al_2Cl_7]^- + LaCl_3 \leftrightarrows La^{3+} + 6\,[AlCl_4]^- \quad (1)$$

reaching maximum solubility of 45 ± 5 mmol kg^{-1} for $LaCl_3$.[73] However, electrodeposition from this solution led to a La content in the alloy deposit below 0.5 at.%. A moderate deposition rate of La was explained by a low La(III) concentration and more negative potentials required for La deposition as compared to that for Al. Moreover, the authors indicated that $[Al_2Cl_7]^-$ anion consumption in the course of Al deposition led to a decrease in solubility of La(III) in the diffusion layer (see reaction 1), complicating the deposition process in this melt.[74] However, Tsuda *et al.*[73] claimed the La deposition in the $[EMIm][Al_2Cl_7]$ IL with the addition of LiCl (3.2 mol kg^{-1}) and $SOCl_2$ (50 mmol kg^{-1}). The addition of thionyl chloride was previously shown to promote the reversible deposition and stripping of alkali metals (Li and Na),[75] and in combination with Li^+ ions the similar effect was expected for La deposition. A cyclic voltammogram displayed only a reduction wave without a respective La oxidation peak. It was proposed that a film that consists of $La(OH)_2$, La_2O_3, LaOCl and $LaCl_3$ was formed in the reaction of the electrodeposited La metal with $SOCl_2$ or residual water in the melt.[73] Thus, this film blocked the oxidation of the La deposit and at the same time also hindered the further La deposition: current values decreased during the electrolysis and reached almost zero after 15 min of deposition. Unfortunately, no microscopic information on the La deposit morphology was provided by the authors.

To increase the lanthanide metal content in the alloy, a highly stable solvate IL comprising a 2 : 1 (mol/mol) mixture of ethylene carbonate (EC) and $AlCl_3$ was employed for electrochemical deposition of a NdAl alloy.[76] The ionic nature of such a solvate IL system results from the reaction (2):

$$2\,AlCl_3 + n\,EC \leftrightarrows [AlCl_2(EC)_n]^+ + [AlCl_4]^- \quad (2)$$

while the introduction of the $NdCl_3$ salt led to its dissolution in the reaction (3):

$$3[AlCl_2(EC)_n]^+ + 2\,NdCl_3 \leftrightarrows 2\,Nd^{3+} + 3[AlCl_4]^- + 3n\,EC \quad (3)$$

This dissolution mechanism was suggested based on Raman and ^{27}Al NMR spectroscopy data.[73, 76] The solubility of $NdCl_3$ achieved in this EC/$AlCl_3$ (molar ratio of 0.667/0.333) solvate IL was as high as 4 mol.% $NdCl_3$. The bulk deposition of NdAl alloy from this solution at 323 K was accomplished, and the obtained deposit contained 30 at.% Nd (according to EDX). Based on cyclic voltammetry, the authors proposed that the electrodeposition of Nd was a direct one-step process.[76]

More recently, Gau and Sun [77, 78] investigated the electrochemical behaviour of Eu and Yb in basic and acidic [EMIm][Cl] – $AlCl_3$ melts with different molar ratios: 0.444/0.556 (prevalent anions are $[AlCl_4]^-$ and Cl^-; a basic melt) and 0.333/0.667 (prevalent anions are $[Al_2Cl_7]^-$; an acidic melt). Since the former system contains some extra Cl^- anions, the dissolution of $EuCl_3$ occurs according to the reaction (4) (same for $YbCl_3$):

$$EuCl_3 + 3\,Cl^- \leftrightarrows [EuCl_6]^{3-} \quad (4)$$

Cyclic voltammetry data demonstrated a reversible one-electron reduction of Eu(III) and Yb(III) to Eu(II) and Yb(II) in the respective IL solutions on a glassy carbon electrode:[77, 78]

$$[EuCl_6]^{3-} + e^- \leftrightarrows [EuCl_4]^{2-} + 2\,Cl^- \quad (5)$$

$$[YbCl_6]^{3-} + e^- \leftrightarrows [YbCl_5]^{3-} + Cl^- \quad (6)$$

No reduction to zero-valent Eu and Yb was observed by Gau and Sun.[77, 78] However, interestingly, the formal potential of the Eu(III)/Eu(II) and Yb(III)/Yb(II) redox couples in the acidic melt was found to be about 2.5 V more positive than the corresponding reactions in the basic melt.[77, 78] Provided that Eu and Yb are dissolved as non-coordinated ions according to the reaction (1),[73, 74] one can assume a crucial role of the coordination sphere around a lanthanide ion in its electrochemical behaviour.[79]

The electrodeposition of Co – Zn – Dy alloy was examined in a low-temperature 50 mol.% – 50 mol.% [EMIm][Cl] – $ZnCl_2$ melt containing 1.687 mol.% $CoCl_2$ and 1.114 mol.% $DyCl_3$ at 373 K.[80] Although energy dispersive X-ray (EDX) analysis showed up to 25 at.% Dy in the deposit, the authors claimed that Dy was mostly deposited in the form of Dy(III) and Dy(II).

The use of the first-generation ILs for lanthanide electrodeposition has an advantage over second-generation ILs due to their lower viscosity (see Table 1) and faster ion diffusion (see Table 2). For example, the diffusion coefficients of Yb(III) ions (estimated from electrochemical data) in [BPy][Cl] – $AlCl_3$ (see [67]) and [EMIm][Cl] – $AlCl_3$ (see [78]) are approximately an order of magnitude larger than those in the second-generation [BMP][TFSI] IL (see Table 2).[81,82] On the other hand, high air- and water-sensitivity is a serious drawback of first-generation ILs. Moreover, despite some successful attempts to deposit lanthanide-based alloy from halometallate ILs, particularly from chloroaluminate ILs, the deposition of pure lanthanides can hardly be realized because of aluminium co-deposition.

3. Deposition from second-generation ionic liquids

Subsequent work on lanthanide electrodeposition was mainly focused on non-halometallate second-generation ILs, especially ILs with the weakly coordinating $[TFSI]^-$ anion, which is typically supposed to provide easier electrodeposition of lanthanides.[83] To increase the lanthanide solubility, the respective salts, $Ln(TFSI)_3$, were synthesized and used.

In particular, [BMP][TFSI] IL was often employed in the studies of lanthanide electrodeposition. This is a rather hydrophobic IL, and it exhibits excellent electrochemical stability at both cathodic and anodic polarization [the electrochemical window is ~4.5 V on Pt (Ref. 84) and ~5.7 V on glassy carbon (GC)[85]]. Suppan *et al.*[86] studied electrochemical deposition of Dy on Au and on sintered Nd – Fe – B permanent magnets from [BMP][TFSI]. The aim of the authors was to enhance the permanent magnetic properties of the Nd – Fe – B magnets. The cyclic voltammograms recorded in 0.147 M $Dy(TFSI)_3$ solution displayed cathodic waves attributed to the reduction of Dy(III) to Dy(0). No respective anodic signal was detected, suggesting the irreversibility of this reaction. Increasing temperature from 298 to 423 K led to an increase in cathodic currents of Dy reduction and to a decrease in the overpotential of this reaction. Galvanostatic deposition of Dy was conducted at -0.5 mA cm^{-2} current density at 423 K. The deposit was characterised by a slightly porous morphology. However, X-ray photoelectron spectroscopy (XPS) analysis after Ar ion sputtering indicated the formation of Dy oxide/hydroxide and a rather low content of metallic Dy (< 1 wt.%).[86] The authors also mentioned that the use of deposition current density of -2 mA cm^{-2} and higher in magnitude resulted in poorly adhesive black deposits and severe IL degradation.

The electrochemical behaviour of Eu was studied in the solution of 53 – 100 mM $Eu(TFSI)_3(H_2O)_3$ in [BMP][TFSI] at 373 K.[85] The cyclic voltammograms of a GC electrode displayed two cathodic peaks at -0.45 (designated as R1) and -2.79 V (R2) *vs.* Fc/Fc^+ as compared to the voltammogram in pure [BMP][TFSI] (Fig. 2 *a*,*b*). Similar peaks were observed on a stainless-steel electrode (Fig. 2 *c*). The first reduction peak R1 was accompanied by a corresponding oxidation peak O1, and this pair of peaks was attributed to a (quasi)reversible one-electron redox process Eu(III) ⇆ Eu(II). In [BMP][TFSI], an additional reduction peak R2 was ascribed to the reduction of Eu(II) to Eu(0) (see Fig. 2). The voltammograms show the difference in the position and the magnitude of the R1 and R2 peaks for GC and stainless steel electrodes. However, because of different

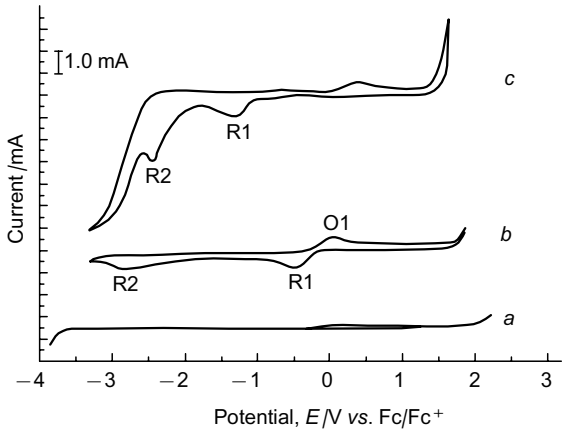


Figure 2. Cyclic voltammograms of [BMP][TFSI] and its solution with $Eu(TFSI)_3$ recorded on GC (*a* and *b*) and stainless steel (*c*) working electrodes at 373 K: (*a*) pure [BMP][TFSI], (*b*) [BMP][TFSI] + 0.053 M Eu(III), (*c*) [BMP][TFSI] + 0.100 M Eu(III). Scan rate: 0.1 V s^{-1}. Reprinted with permission from Ref. 85.

Eu(III) concentrations in the two measurements (0.053 *vs* 0.100 V), it is not clear whether the changes in voltammetric features were related to the different Eu(III) concentrations or to the electrode material. After five-hour potentiostatic polarization of the GC and stainless steel electrodes at the potentials of possible Eu deposition, the samples were analyzed *ex situ* by energy dispersive X-ray fluorescence (EDXRF) spectroscopy and X-ray diffraction (XRD) spectroscopy. The EDXRF and XRD spectra showed the presence of metallic Eu; however, neither further details on deposit composition nor deposit morphology data were presented in this study.[85]

Hussey and co-workers introduced Ce, Eu, Sm, Yb, Nd, Pr ions into [BMP][TFSI] by the anodic dissolution of the corresponding metals.[81,87,88] The oxidation state of the lanthanide ions in the bulk was examined by electronic absorption spectroscopy, and electrochemical behaviour was studied by cyclic voltammetry at 323 K. Based on the results, Hussey *et al.* proposed that Ln(III) (here Ln = Nd, Pr and Ce) were reduced to divalent ions during the cathodic scan, but the resulting divalent species exhibited only transient stability [with Sm(II) being somewhat less stable as compared to other lanthanides[81]] undergoing rapid disproportionation to Ln(III) and Ln(0):[87,88]

$$Ln(III) + e^- \leftrightarrows Ln(II) \quad (7)$$

$$2\,Ln(II) \rightarrow Ln(III) + Ln(0) \quad (8)$$

This Ln(II) disproportionation reaction was often observed in chloride melts at high temperatures.[89,90] The Ln(0) can further react with components of the IL to form a passivating film on the electrode surface as also observed in the course of deposition of some metals, *e.g.* Li or Cr, in ILs and DESs.[91–94] However, the presence of an anodic peak in CV curves,[81,87,88] corresponding to oxidation of Ln(II) to Ln(III), indicates that the disproportionation reaction (8) is rather slow. Moreover, Yamagata *et al.*[82] demonstrated quasireversible redox transformations between three- and divalent Ln ions in [BMP][TFSI] and [EMIm][TFSI], and no evidence was found for the disproportionation of Eu(II), Yb(II) and Sm(II) at 298 K. Bourbos *et al.*[95] studied the

deposition of several Ln (Ln = La, Sm, Nd and Dy) from [BMP][TFSI] and $[N_{1,1,1,4}][TFSI]$ at room temperature. The disproportionation reaction (8) was not considered in this work. Instead, the authors claimed the irreversible three-electron reduction of Ln(III) to Ln(0) based on CV, scanning electron microscopy (SEM), EDX and XPS data, however, no evidence for or against the disproportionation reaction was given. Nevertheless, the disproportionation reaction was suggested to occur for Sm(II) at 373 K, when it was formed upon Sm(III) electroreduction in [BMP][TFSI].[96] The cyclic voltammograms at 50 to 200 mV s^{-1} showed both cathodic and anodic peaks corresponding to Sm(III) ⇆ Sm(II) reactions, whereas at the scan rate of 10 mV s^{-1} anodic peak disappeared.[96] At 298 K, the anodic peak was still present in voltammograms recorded at 10 mV s^{-1}. These findings indicate that the disproportionation reaction (8) is slow and accelerates with temperature.

An interesting approach was employed by Hatchett *et al.*,[97] to obtain a solution of Ce(III) in $[N_{1,1,1,4}][TFSI]$ IL. The ILs that are based on quaternary ammonium cations also exhibit a wide electrochemical window (> 4.5 V).[57, 98] Carbonate hydrates $Ce_2(CO_3)_3 \cdot x\,H_2O$ were dissolved in the solution of H[TFSI] acid in $[N_{1,1,1,4}][TFSI]$ according to the following reactions (the dissolution was confirmed by UV-Vis and IR spectroscopy):[97]

$$Ce_2(CO_3)_3 \cdot x\,H_2O + 6\,H[TFSI] \rightarrow \quad (9)$$
$$\rightarrow 2\,Ce(TFSI)_3 + 3\,CO_2 + (3 + x)H_2O$$

or

$$Ce_2(CO_3)_3 \cdot x\,H_2O + 10\,H[TFSI] \rightarrow \quad (10)$$
$$\rightarrow 2\,Ce(TFSI)_5^{2-} + 4\,H^+ + 3\,CO_2 + (3 + x)H_2O$$

The cyclic voltammograms of Au, Pt and GC electrodes in this solution displayed the multiple voltammetric features at potentials below 1 V *vs* Ag/AgCl (~0.6 V *vs* Fc/Fc^+ according to Ref. 99; hereinafter, this conversion is quite approximate, since it may considerably depend on the solution composition and the reference electrode configuration and composition). The authors indicated that water was still present in the IL solution despite the degassing of the latter by Ar for 24 h. Due to the presence of water, some voltammetric features were related to the reduction of water and oxidation of the electrode surfaces. Moreover, since H[TFSI] was added in excess [as compared to the stoichiometry of reactions (9 and 10)], H[TFSI] could also be a proton donor for HER. Although the authors ascribed some voltammetric features to consecutive one-electron reactions

$$Ce(TFSI)_{3,ads} \rightarrow Ce(TFSI)_{2,ads} \rightarrow Ce(TFSI)_{ads} \rightarrow Ce(0)_{ads} \quad (11)$$

as well as to the three-electron reaction

$$Ce(TFSI)_3 + 3e^- \rightarrow Ce(0)_{ads} + 3\,TFSI^- \quad (11a)$$

this interpretation of the voltammetric responses was based only on a comparison of cyclic voltammograms in the presence and in the absence of the Ce(III) salt and was not supported by other methods. A deposit obtained on Au in the course of the potential sweep was non-uniform and covered the Au surface only partially (as shown by SEM).

Irreversible three-electron reduction of La(III) to La(0) was evidenced by voltammetric measurements in 66 mM $La(TFSI)_3(H_2O)_3$ in $[N_{1,1,1,4}][TFSI]$.[100] Bhatt *et al.*[100] stated that La had only one stable oxidation state (+III) in addition to zero and ruled out the possibility of the La(III) → La(II) process. On the contrary, the reduction of Eu(III) and Sm(III) to Eu(0) and Sm(0), respectively, occurred *via* the formation of divalent ions. The CV curves displayed redox peaks ascribed to (quasi)reversible Eu(III) ⇆ Eu(II) and Sm(III) ⇆ Sm(II) processes and irreversible cathodic waves at more negative potentials attributed to Eu(II) → Eu(0) and Sm(II) → Sm(0).

The deposition of La was also realized in [OMP][TFSI], where La was introduced as $La(NO_3)_3$.[56] The CV curves of a platinum electrode displayed only one pronounced cathodic wave ascribed to the reduction of La(III) to La(0). Potentiostatic electrodeposition of La was performed with or without stirring at varied potentials using La(III) concentrations ranging from 5 to 500 mM and temperatures ranging from 298 to 353 K.[56] Best quality deposits were obtained from a 60 mM La(III) solution at −1.5 V *vs* AgCl-covered Ag wire pseudo-reference electrode at room temperature and without solution agitation. The SEM, EDX and XRD experiments revealed an amorphous La deposit with a granular morphology. The authors stated that the use of more negative potentials, higher La(III) concentrations and temperature above 313 K accelerated the deposition rate, but led to the cracking and peeling of the deposit. The amorphous state of the La deposit[56] can be due to the inclusion of the light elements (O, S, F, N) and metalloid (C) into the deposits as previously discussed in the literature.[101, 102] The presence of these elements can be explained by parallel side reactions of cathodic IL or DES component decomposition as well as chemical oxidation of deposited lanthanides in the presence of residual water.

A number of studies on lanthanide electrodeposition employed ILs with quaternary phosphonium cations, particularly $[P_{2,2,2,5}][TFSI]$ that exhibited relatively low viscosity (see Table 1) and comparable or even larger electrochemical windows than $[N_{1,1,1,4}][TFSI]$ and [BMP][TFSI] ILs.[58, 103] The electrochemical reduction of Dy was investigated from 0.075 and 0.1 M $Dy(TFSI)_3$ in $[P_{2,2,2,5}][TFSI]$ IL at elevated temperature (318 to 378 K) on a Pt working electrode.[104, 105] The cathodic peaks R1 and R2 at about −2.4 and −3.4 V *vs* Fc/Fc^+ were attributed to the irreversible Dy(III) → Dy(II) and Dy(II) → Dy(0) reduction processes (Fig. 3 *a*). In the presence of slightly higher water content (203 ppm), however, the peak R1 was absent and the peak R2′ was assigned to three-electron reduction of Dy(III). This difference in the behaviour was explained by preferential coordination of Dy(III) ions with water molecules upon an increase in water content.[105] The deposition of Dy was performed on a copper plate cathode with a Dy rod as an anode in two-electrode cell configuration at a constant cell voltage of −3.8 V at 373 – 423 K.[104] Based on the gravimetric analysis (by weighting the Cu cathode and the Dy anode before and after deposition), the authors claimed current efficiency of 75% – 78% for Dy deposition and dissolution.[104] The deposit obtained at 423 K was characterized with SEM: the surface morphology was granular with cracks and with a particle diameter of 0.5 μm. Although the deposition was performed under air atmosphere, EDX and XRD analysis showed a pure bulk Dy metal deposit (except for the top layer) rather than Dy_2O_3. The nucleation and growth of the Dy deposit were explored in a series of potentiostatic current transients (Fig. 3 *b*).[105] The 'cathodic current density *vs* time' plots initially increased due to a growing area of nuclei, and then the cathodic current dropped because of diffusion limitations (overlapping of diffusion zones around nuclei) (see Fig. 3 *b*).

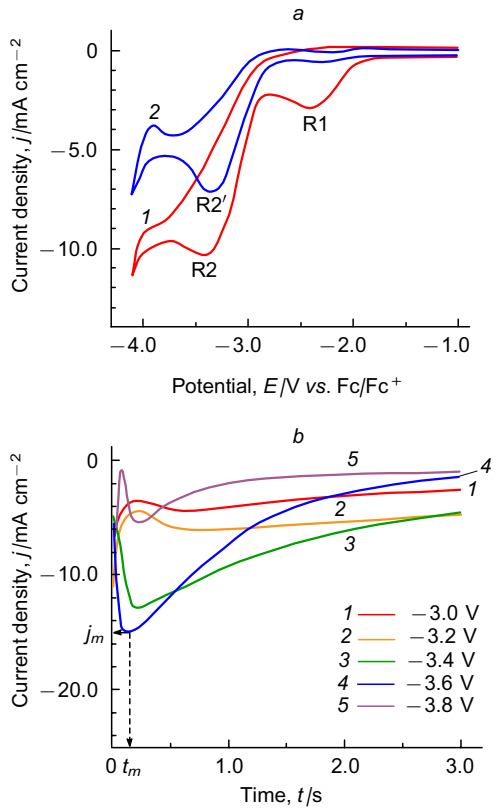


Figure 3. (*a*) The cyclic voltammograms of a Pt electrode in 0.1 M Dy(III) + $[P_{2,2,2,5}][TFSI]$ at 363 K with different water content, (*1*) 98 ppm and (*2*) 203 ppm. (*b*) Chronoamperograms recorded on a Pt electrode in 0.1 M $Dy(TFSI)_3$ + $[P_{2,2,2,5}][TFSI]$ at 363 K. Reprinted with permission from Ref. 105.

Based on the analysis of the transients, the authors suggested that the Dy(0) nucleation mechanism changes from instantaneous nucleation to progressive nucleation with increasing overpotential. A similar nucleation mechanism was also observed by the same research group for the deposition of Nd from the [DEMMA][TFSI] IL.[106] The deposition of Nd from [DEMMA][TFSI] produced a deposit with a granular morphology with a non-uniform grain size distribution. The XPS analysis, performed after the Ar ion beam sputtering (to facilitate in-depth analysis of the middle layer) identified the deposits as mixtures of Nd metal and Nd oxide.[106] The authors suggested that metallic Nd was initially electrodeposited and further *in situ* oxidized by the oxygen components in the electrolyte, that is, water or dissolved oxygen.

The deposition of Nd from a phosphonium-type IL was attempted by Kondo *et al.*[107] A solution with a high concentration (0.5 M) of $Nd(TFSI)_3$ in the $[P_{2,2,2,5}][TFSI]$ IL was employed to test Nd deposition on Pt and Cu substrates at elevated temperatures. A cathodic peak at ~ -2.5 V *vs* Fc/Fc^+ was ascribed to the reduction of Nd(III) to Nd(0), while an anodic peak at 0.5 to 1.0 V (depending on the temperature) was attributed to the opposite oxidation reaction. Because of a large width of the redox peaks and a large peak-to-peak separation (> 2.8 V), it was conjectured that the redox reaction of Nd(III)/Nd(0) should be regarded as an irreversible system. The increase in temperature from 323 to 378 K led to a decrease in overpotentials for both Nd(III) reduction and Nd(0) oxidation. However, the reductive decomposition of IL was also accelerated at higher temperatures. The deposit obtained at −3.1 V over 3 h was not compact and represented grains with an average size of 1.7 μm. The content of metallic Nd was estimated by EDX to be 48% (the authors did not specify if it was atomic percentage or percentage by weight). Since oxygen was also detected, it was proposed that the oxidation reaction in the top layer of electrodeposits could occur in the course of the electrodeposition.[107] Although Kondo *et al.*[107] demonstrated a successful deposition of Nd from $[P_{2,2,2,5}][TFSI]$ (dynamic viscosity is 88 mPa s,[58] see Table 1), no Nd deposition was detected by the same authors in more viscous $[N_{1,1,1,6}][TFSI]$ [dynamic viscosity is 153 mPa s (Ref. 57)]. The authors concluded that the viscous IL was likely to cause a decrease in the ionic mobility and the diffusion coefficient of Nd(III), which in turn hindered the reduction of Nd(III).

Additionally, the deposition of Nd from the $[P_{2,2,2,5}][TFSI]$ IL was studied with a combination of electrochemical methods (CV and CA) and EQCM (electrochemical quartz crystal microbalance) technique.[108] The EQCM technique allowed the detection of changes in the mass (Δm) of electrodeposits on the electrode and in the viscosity and density of the electrolyte near the electrode ($\Delta\eta\rho$), which is related to the concentration of soluble metal ions in ILs. The EQCM data were measured simultaneously with CV in a 0.05 M Nd(III) + $[P_{2,2,2,5}][TFSI]$ solution at different temperatures (Fig. 4 shows the data for 373 K). A clear increase in the deposit mass was observed at potentials < −2.4 V, which corresponded to the cathodic voltammetric peak (Fig. 4 *a*,*b*). These observations were assigned to the reduction of Nd(III) to metallic Nd(0):

$$[Nd(TFSI)_5]^{2-} + 3e^- \rightarrow Nd(0) + 5\,TFSI^- \qquad (12)$$

The calculated molecular mass, M_{app}, of the electrodeposited Nd (calculated from the mass change Δm according to Faraday's law of electrolysis) was equal to 140.4 in the potential range between −2.4 and −2.9 V (Fig. 4 *b*) and close to the theoretical value of M_{app} for the electrodeposition reaction of Nd(III)/Nd(0), *i.e.* 144.2 g mol^{-1}. An increase in the mass and in M_{app} at potentials between 0.0 and −2.0 V (Fig. 4 *b*) was ascribed to the formation of Nd(II), followed by the disproportionation reaction (8). Another reason for the increase in the mass was proposed to be the formation of a film on the electrode surface as observed for Li in ILs.[109] The decrease in parameter $\eta\rho$ (here η is the dynamic viscosity and ρ is the density of the solution adjacent to the working electrode) at potentials between −2.4 and −2.8 V correlated well with the consumption of Nd(III) ions (Fig. 4 *c*), which in turn should lead to a decrease in the viscosity.[108] However, increasing $\eta\rho$ at more negative potentials indicated that the Nd(III) reduction reaction (12) competed with IL degradation. The formation of a Nd electrodeposit was also confirmed by EQCM under potentiostatic conditions at −3.2 V.[108] Further, the obtained blackish deposit was characterized by SEM, EDX and XPS. According to the EDX analysis, the deposit contained 85.7 wt.% Nd and such elements as C, O, F, N, P derived from the IL, while XPS confirmed the primarily metallic state of Nd in the middle deposit layer at a depth of 0.08 – 0.15 μm. The content of metalloids such as C (1.02 wt.%) and P (0.02 wt.%) was not considerable and could hardly affect the deposit crystallinity. The crystallinity of the Nd deposit obtained in $[P_{2,2,2,5}][TFSI]$ was confirmed by XRD by Kazama *et al.*[105] On the other hand, the

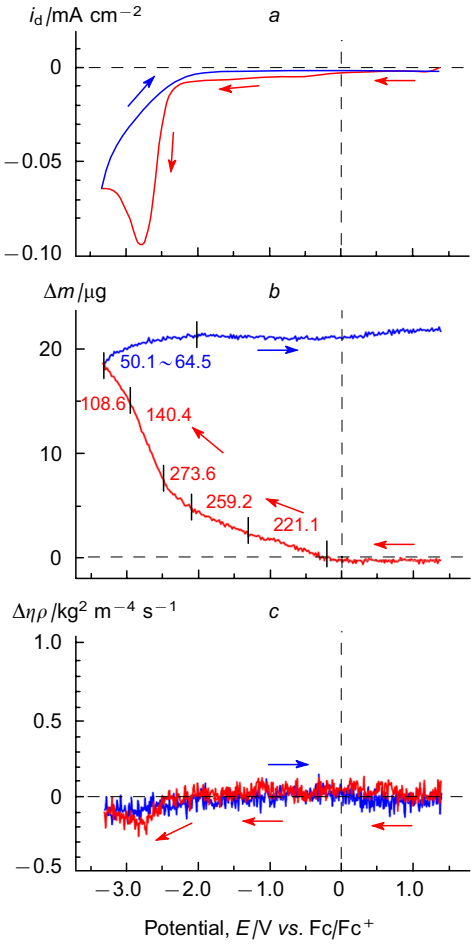


Figure 4. CV/EQCM analysis of 0.05 M Nd(III) in [$P_{2,2,2,5}$][TFSA] at 373 K at a scan rate of 2 mV s^{-1}; (*a*) the voltammogram, (*b*) the mass change (the values indicate M_{app}/g mol^{-1}) and (*c*) the change in $\eta\rho$ values. Reprinted with permission from Ref. 108.

content of O exceeded 8 wt.%, suggesting partial lanthanide oxidation (with formation of oxides and hydroxides).

It is worth noting the following observations. The diffusion coefficients of Ln(III) species in the most studied [BMP][TFSI] and [$P_{2,2,2,5}$][TFSI] ILs were estimated to be of an order of $\sim 10^{-12}$ m^2 s^{-1} at room temperature or slightly above room temperature (see Table 2). These diffusion coefficients were less than half of those of Fe(II) (Ref. 110) and Co(II) (Ref. 111) in [BMP][TFSA], which can be explained by the difference in coordination environment of the species. Particularly, Co(II) was considered to be the octahedrally coordinated complex $[Co(TFSA)_3]^-$,[112,113] while Yb(II) was reported to form $[Yb(TFSA)_4]^{2-}$.[79,114] Assuming that Eu(II) species form a complex similar to that of Yb(II), Tachikawa *et al.*[115] concluded that the small diffusion coefficient of Eu(II) was due to the larger size and charge of the species. The Ln(III) ions are typically coordinated with five $[TFSI]^-$ anions (as estimated from Raman spectroscopy[116]) and the diffusion coefficients of Ln(III) are similar or even lower than those of Ln(II) species.

The presence of water in ILs may crucially affect bulk properties of IL solutions,[117] speciation of metal ions and electrode/IL interface structure as shown in experimental[118] and modelling studies.[119] Thus, water may significantly affect the kinetics and mechanism of metal ion electroreduction. Regarding lanthanide deposition, an increase in water content may affect the hydration states of Ln(III) ions in ILs, increase Ln salt solubility, change the kinetics of Ln(III) reduction, improve mass transport and induce different side reaction (HER, IL reductive degradation).[120] The effect of water in [TFSI]-based ILs on the electrochemical behaviour and deposition of lanthanides was investigated by different research groups. Kondo *et al.*[121] concluded that even a moderate water content (~2300 ppm) in a 0.5 M $Nd(TFSI)_3$ solution in the [$P_{2,2,2,5}$][TFSI] IL only slightly improved the viscosity and electrical conductivity, but noticeably increased the overpotential for Nd(III) reduction. The latter negative effect was explained by the stabilization of the Nd(III) complexes by water molecules. Yet, no significant influence of the moderate water content on the oxidation state of Nd deposit was observed. In both cases, in dehydrated solution and solution with ~2300 ppm water, the deposit contained mostly Nd in the metallic state.[121] An inhibitory effect of small water amount was also observed for the reduction of Dy(III) in [$P_{2,2,2,5}$][TFSI] (see Fig. 3 *a*).[105]

Sanchez–Cupido *et al.*[122] came to an opposite conclusion on the water effect. They studied the electrodeposition of Nd from [$P_{6,6,6,14}$][TFSI] IL and found that the Nd(III) reduction is accelerated in the presence of 0.4 wt.% water as compared with the solution containing 0.1 wt.% water. Although the IL cations were different in the two papers, $[P_{2,2,2,5}]^+$ (Ref. 121) and $[P_{6,6,6,14}]^+$ (Ref. 122), the opposite water effect can hardly be explained by the difference in cations, and a further examination is required.

The effect of water on the electrochemical properties of lanthanides in ILs was also investigated by Nagaishi *et al.*[60] The authors studied coordination states and electrochemical behaviour of Eu(III) ions in dehydrated and water-saturated ILs, [DEMMA][TFSI] [DEMMA is *N*,*N*-diethyl-*N*-methyl-*N*-(2-methoxyethyl)ammonium] and [BMIm][TFSI]. It was stated that Eu(III) was coordinated only with water molecules in water-saturated ILs. Nevertheless, the quasireversible redox process Eu(III)/Eu(II) in [DEMMA][TFSI] and [BMIm][TFSI] was shifted to more positive potentials as compared with the formal potentials in an aqueous solution.[60] This shift was particularly pronounced in dehydrated ILs. For example, the formal potential of Eu(III)/Eu(II) in dehydrated [DEMMA][TFSI] was 0.75 V more positive than that in the aqueous solution. This finding suggests that Eu(II) ions are more stable in ILs than in aqueous solutions. However, it is not clear how the authors accounted for the changing liquid-junction potential between the reference electrode (aqueous) and the IL solution when they compared the potentials with aqueous electrolyte solutions. The diffusion coefficients of Eu(III) estimated in water-saturated and dehydrated [DEMMA][TFSI] and [BMIm][TFSI] ILs as well as in an aqueous solution are given in Table 2.[60] Although the diffusion coefficient of Eu(III) in both ILs increases by a factor of 3–4 upon saturation with water (*e.g.* from 2.3×10^{-12} to 8.9×10^{-12} m^2 s^{-1} in [BMIm][TFSI], see Table 2), it is still much smaller than the diffusion coefficient of Eu(III) in the aqueous solution (1.6×10^{-9} m^2 s^{-1}). It was also pointed out that the diffusion coefficient of Eu(III) estimated from electrochemical data was much lower than that estimated from the viscosity of ILs,[60] which can be explained by the effective inhibition of motion of Eu(III) by the matrix of IL. The formation of a pronounced anion-cation layering at the metal/IL interface has been demonstrated previously.[118,123–125] This a layering may change the physical

properties of IL at the interface: *e.g.*, the viscosity might locally change by 1 to 3 orders of magnitude as reported in the literature.[126, 127] Thus, the mass transport of lanthanide ions can be decelerated substantially in a near-surface IL layer as compared to the bulk IL.

Triflate-based ILs (with $[OTf]^-$ anion) are another type of ILs with a relatively large electrochemical window (> 4 V).[128, 129] However, although $Ln(OTf)_3$ salts are relatively inexpensive and commercially available and may have appreciable solubility in triflate-based ILs, the study of lanthanide deposition from these ILs is limited. One of the reasons can be the higher viscosity of triflate ILs as compared to [TFSI]-based ILs (see Table 1). The electrodeposition of Y, Gd and Yb was studied by cyclic voltammetry in three ILs, $[N_{1,4,4,4}][OTf]$, [BMP][OTf] and [BMMIm][OTf] (BMMIm is 1-butyl-2,3-dimethylimidazolium), on copper and platinum electrodes.[130] The authors observed no voltammetric signals of lanthanide deposition in [BMMIm][OTf], while the cathodic waves appearing in $[N_{1,4,4,4}][OTf]$ and [BMP][OTf] were ascribed to the reduction of Ln(III) to Ln(II) followed by the further reduction to Ln(0). However, neither microscopic nor spectroscopic characterization of lanthanide deposits was provided.

The voltammetric behaviour of some lanthanides was also studied in [Cl]-based ILs. Quasireversible redox peaks for Eu(III)/Eu(II), Sm(III)/Sm(II) and Ce(III)/Ce(II) were observed in [EMIm][Cl] and [BMIm][Cl] IL at 343 – 398 K.[131, 132] However, lanthanide deposition in these ILs was not studied, since severe reductive IL degradation proceeded at potentials prior to the reduction of lanthanides to the zero-valent state.

Recently, low-viscosity ILs with $[DCA]^-$ anions (see Table 1) were employed for lanthanide electrodeposition. Zhang *et al.*[133] reported on the deposition of La from [BMIm][DCA] at 333 K. Although it is known that metal chlorides are poorly soluble in many non-chloroaluminate ILs, appreciable solubility of anhydrous $LaCl_3$ (at least up to 80 mM) was achieved in [BMIm][DCA] due to good donor ligand properties of $[DCA]^-$.[62] Based on the amperometric titration results, the following dissolution reaction was proposed:

$$4[DCA]^- + LaCl_3 \rightarrow [La(DCA)_4]^- + 3\,Cl^- \qquad (13)$$

In agreement with the above-mentioned studies,[56, 100] Zhang *et al.*[133] also observed a single cathodic wave and attributed it to the reduction of La(III) to La(0) in [BMIm][DCA]. Interestingly, the anodic peak of deposit stripping was also observed in the reverse scan of CV. Though this anodic peak was much less pronounced than the cathodic one, it can be ascribed to partial oxidation of La(0). The anodic counter peak was not observed in other reports,[56, 85, 100, 104, 130] where La (and other lanthanides) were deposited irreversibly from $[TFSI]^-$- and $[OTf]^-$-based ILs. Zhang *et al.*[133] performed potentiostatic deposition of La from a 0.08 M La(III) solution in [BMIm][DCA] on a Pt foil electrode at different potentials at 333 K. The XRD and XPS analysis of the La deposit demonstrated that the surface of the substrate was originally covered by a thin lanthanum layer. Although La_2O_3 was detected on the surface, it can be explained by the oxidation of the freshly deposited La when exposed to the ambient atmosphere. Nevertheless, the chemical oxidation of La(0) upon deposition cannot be excluded from the reported results.

The SEM analysis showed a clear influence of the deposition potential on the deposit morphology (Fig. 5). At rather a moderate overpotential, namely at −0.9 V *vs* Ag/Ag^+ reference electrode (*ca.* −1.43 V *vs* Fc/Fc^+; according to Ref. 134 the formal potential of Fc/Fc^+ in ILs is ~0.53 V *vs* Ag/Ag+ in acetonitrile solution), the La deposit represented 150 – 200-nm nanoparticles (Fig. 5 *a*,*e*), suggesting the formation of a limited number of nuclei in the nucleation stage and their further growth. At −1.0 V, the deposit became more compact (Fig. 5 *b*,*f*); however, at more negative potentials, the deposit appeared like a disordered porous and dendritic structure (Fig. 5 *c*,*d*,*g*,*h*). The results of this study suggest that the [DCA]-based ILs are promising media for electrochemical deposition of lanthanides and other elements. However, the surprisingly low diffusion coefficient of La(III) in [BMIm][DCA] was calculated from electrochemical data (1.21×10^{-14} $m^2\ s^{-1}$ at 333 K).[133] This value is much smaller than the typical values estimated by other groups for other lanthanides (see Table 2): *e.g.* it is three orders of magnitude smaller than the diffusion coefficient of Eu(III) in the same IL (26.5×10^{-12} $m^2\ s^{-1}$).[63] Such a low value may result from

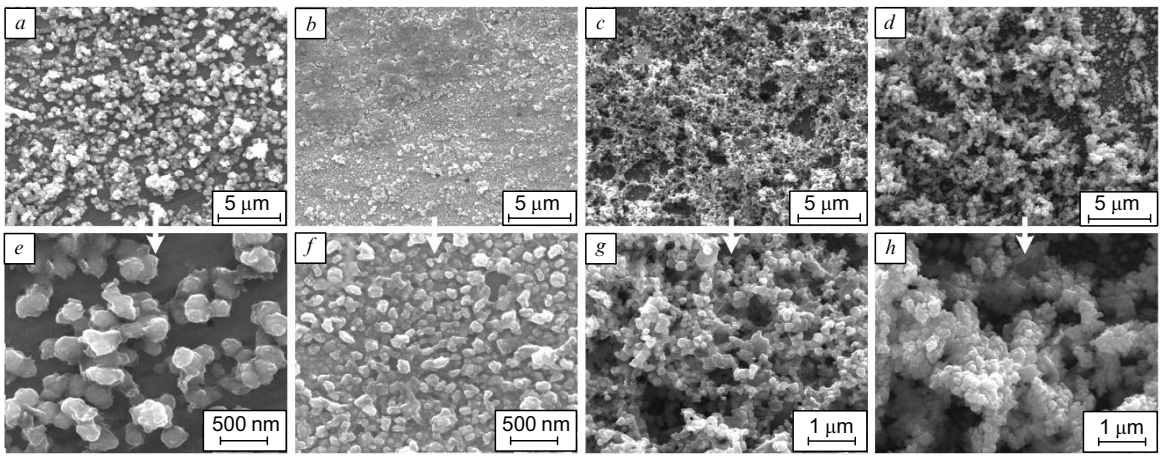


Figure 5. SEM images of lanthanum electrodeposited on Pt foil in 0.08 M $LaCl_3$/[BMIm][DCA] IL at the applied potentials of (*a*) −0.90 V, (*b*) −1.00 V, (*c*) −1.05 V and (*d*) −1.10 V for 2 h at 333 K, respectively. (*e*−*h*) The corresponding high-magnification SEM images. Reprinted with permission from Ref. 133.

a mistake in the diffusion coefficient calculation and has to be rechecked.

The [BMIm][DCA] IL was also employed as a medium for electrodeposition of Gd at 330 – 333 K from a 0.08 M $GdCl_3$ solution.[135] The voltammetry, chronoamperometry and EQCM data suggested the deposition of a Gd film, which could be seen with the eye. However, no microscopic and elemental analyses were performed to investigate the morphology and composition of the film.

Electrochemical deposition of Er (one of less studied lanthanides) was investigated by Small *et al.*,[12] who employed different ILs ($[N_{1,1,1,4}]$[TFSI], [MPP][TFSI], [BMP][TFSI], [BMP][DCA], [BMP][OTf], where MPP is 1-methyl-1-propylpiperidinium) and introduced Er(III) to the ILs as $Er(OTf)_3$ or $Er(TFSI)_3$. Voltammetry data showed an intermediate reduction process on a Pt electrode before the reduction of Er(III) to Er(0) in the $[TFSI]^-$- and $[OTf]^-$-based ILs. However, the product generated in this intermediate process was not specified. Among the studied ILs, [BMP][DCA] was shown to provide optimal conditions for Er deposition: the absence of the intermediate reduction process and higher reduction currents on the Pt electrode. However, the presence of metallic Er in the deposit was open to question, as followed from XPS and EDX analyses of the films obtained by potentiostatic deposition at −2.9 V *vs* Fc/Fc^+ for 2 h.[12] Interestingly, Small *et al.* found out that the activity of electrodes towards Er(III) reduction depended on the electrode material: *e.g.* the activity of a gold electrode was similar to that of Pt, while no Er(III) reduction was detected on GC.

Thomas *et al.*[136] attempted to prepare functional materials for optoelectronic applications by electrochemical co-deposition of Si and Er or Tb lanthanides with highly efficient light emission. Co-deposition of Er or Tb with Si was performed from the [BMP][TFSI] IL solutions containing 10 mM $ErCl_3$ or $TbCl_3$ as well as $SiCl_4$. ~2 μm-thick films were obtained with different content of Er or Tb (from 5 at.% to 20 at.%) at 343 K. Moreover, the authors succeeded in depositing pure Er and Tb films. The EDX and SIMS (Secondary Ion Mass Spectrometry) analyses confirmed the lanthanide deposition.[136] However, rather strong oxygen signals were also observed, suggesting that Er and Tb were, at least partially, in an oxide form in the deposit.

Berger *et al.*[137] employed IL with a hexaalkyl-substituted guanidinium cation to deposit Dy on the Au(111) single crystal surface. The $Dy(OTf)_3$ salt was dissolved in $[N_{1,1}N_{1,1}N_{pip}Gua]$[TFSI] (see the cation structure in Fig. 1) to obtain 0.02 to 0.20 M solutions. The deposition of Dy was concluded from CV data and *in situ* STM data. The STM imaging displayed the formation of monoatomic high islands on the Au terraces at the potentials of a cathodic wave. The XPS spectra show signals that were ascribed to Dy_2O_3; however, it is not clear if the oxidation of Dy(0) can take place during sample transfer to the XPS device or Dy oxidation can occur upon electrodeposition.

Recently Nockemann and co-workers[138] synthesized and characterized IL chlorometallate complexes using the $[P_{6,6,6,14}]^+$ cation for the whole lanthanide series (Ln = La, Ce, Pr, Nd, Sm, Eu, Gd, Tm, Tb, Dy, Ho, Er, Yb, Lu) and two other rare-earth elements, Sc and Y, with melting points below 273 K. The ILs of the $[P_{6,6,6,14}]_3[LnCl_6]$ type were obtained in such reactions as:

$$3[P_{6,6,6,14}]Cl + LnCl_3 \rightarrow [P_{6,6,6,14}]_3[LnCl_6] \quad (14)$$

or

$$3[P_{6,6,6,14}]Cl + LnCl_3 \cdot 6\,H_2O \rightarrow [P_{6,6,6,14}]_3[LnCl_6] + 6\,H_2O \quad (15)$$

The electrochemical behaviour of $[P_{6,6,6,14}]_3[LaCl_6]$ (melting point is ~271 K) was investigated in this paper by cyclic voltammetry at elevated temperatures (383, 393 and 403 K).[138] The cathodic peak at −1.5 V *vs* Ag/Ag^+ (a silver wire immersed in 0.01 M $AgNO_3$ solution in $[BMIm][NO_3]$) and the anodic peak-like feature at ~0.3 V *vs* Ag/Ag^+ were attributed to the reduction/oxidation of the La(III)/La(II) redox couple. Although the authors assumed the existence of La(II) species in a chloride-rich chlorolanthanate environment, one could think that the disproportionation reaction (8) was feasible in this IL system.[87,88] Apparently, chloride as a strong complexing ligand hindered the electroreduction of the $[LaCl_6]_3^-$ species,[138] whereas a dicyanamide complex of lanthanum favoured electroreduction of La(III) species.[133]

Already a few decades ago, it was found by several research groups[139,142] that lanthanide halides formed complexes with a number of electron donor compounds, in particular organic phosphorus and sulfur compounds such as tributyl phosphate (TBP) or diamyl sulfoxide. Recently, following this strategy, Bagri *et al.*[143] prepared an ionic liquid system by dissolving $Ln(TFSI)_3$ salts in trimethyl phosphate (TMP). This ionic system was later called *neutral-ligand ionic liquid* (NLIL).[144] Bagri *et al.*[143] stated that upon the dissolution, Ln formed a complex cation with the neutral TMP ligands:

$$3\,TMP + Ln(TFSI)_3 \rightarrow [Ln(TMP)_3]^{3+} + 3[TFSI]^- \quad (16)$$

The complex cation composition was proposed by analogy with previously reported lanthanide complexation with TBP,[139] where the composition was determined by infrared spectroscopy measurements. In this system, the electrochemical deposition of Pr, Gd, Dy and Nd was studied from solutions containing 0.15 to 0.22 M of respective $[Ln(TMP)_3]^{3+}$ ions at room temperature.[143] The authors claimed the deposition of Ln(0) on the basis of CV and SEM/EDX mapping characterization. However, the oxidation state of Ln in the deposit was not analyzed. Since the solutions contained about 4000 ppm water, the Ln oxide/hydroxide formation could take place. Diffusion coefficients of Ln(III) complex cations were estimated from CV data to be of an order of 10^{-13} to 10^{-14} $m^2\,s^{-1}$, which was significantly lower than the typical values ($> 10^{-12}$ $m^2\,s^{-1}$) for Ln(III) in [TFSI]- and [DCA]-based ILs (see Table 2). Such low values of diffusion coefficients might be due to low viscosity; however, the authors did not report the viscosity of the Ln(III)-containing solution.

Matsumiya *et al.*[145] studied the extraction of Ln(III) (Ln = Nd, Pr, Dy) from a Ln(III)-containing waste solution in water by complexation of Ln(III) with the TBP neutral ligand dissolved in the $[P_{2,2,2,4}]$[TFSI] IL. The concentration change was monitored by inductively coupled plasma atomic emission spectroscopy. The extraction of Ln(III) was shown to proceed according to a cation-exchange mechanism between aqueous and IL phases:

$$Ln_{aq}^{3+} + 3TBP_{IL} + [P_{2,2,2,4}][TFSI]_{IL} + 2[TFSI]^- \rightarrow \quad (17)$$
$$\rightarrow [Ln(TBP)_3]^{3+}[(TFSI)_3]_{IL}^{3-} + [P_{2,2,2,4}]_{aq}^+$$

The structure of Ln the complex ion was suggested based on the lanthanide extraction data and Raman spectroscopy.[145]

Further, the reduction of $Nd(TBP)_3^{3+}$ in $[P_{2,2,2,4}][TFSI]$ to Nd(0) was confirmed by CV analysis and potentiostatic deposition of a thick Nd film at 373 K.[145] The electrodeposited Nd was investigated by XPS. The $Nd3d_{5/2}$ spectra for the top surface and the middle layer of the electrodeposits are shown in Fig. 6. The $Nd3d_{5/2}$ peaks for the Nd metal and oxides are positioned at 980.5–981.0 eV and 981.7–982.3 eV, respectively. Upon Ar etching, the observed $Nd3d_{5/2}$ peak shifted to a lower binding energy of 980.5 eV, *i.e.* to the theoretical binding energy of the Nd metal (see Fig. 6). The C and O bonding peaks were also detected, but their intensity decreased gradually with increasing depth of Ar etching. Based on these results, Matsumiya *et al.*[145] suggested that the middle and surface layers of Nd electrodeposits were in the metallic state and partially in the oxidized state, respectively. However, it should be note that the broadness and asymmetry of XPS peaks before and after Ar etching (see Fig. 6) may be indicative of the presence of Nd oxide form in the middle layer as well (at least to a certain extent). Rather similar results were obtained by the same research group for extraction and deposition of Nd(III), Pr(III) and Dy(III) using the *N*,*N*,*N*′,*N*′-tetraoctyl diglycolamide (TODGA) neutral ligand.[146]

Inspired by the idea of Bagri *et al.*,[143] Krishna *et al.*[144] used another neutral ligand, *N*,*N*-dihexyl octanamide (DHOA) to prepare NLILs with $Ln(TFSI)_3$ (Ln is Eu, Dy, Nd). The formation of $[Ln(DHOA)_3]^{3+}[(TFSI)_3]^{3-}$ [similarly to the reaction (16)] upon dissolution of $La(TFSI)_3$ in DHOA was proposed based on CV and infrared spectroscopy data. Cyclic voltammograms recorded in 0.1 M $Ln(TFSI)_3$ in DHOA exhibited the responses attributed to the reduction of Ln(III) to Ln(0). Furthermore, Nd(III) and Dy(III) were reduced in a single three-electron step, while the reduction of Eu(III) proceeded in two steps *via* the formation of Eu(II) species.[144] Diffusion coefficients were estimated to be on an order of 10^{-12} m^2 s^{-1}, similar to those in [TFSI]-based ILs (see Table 2).

As can be seen in the cited literature, the deposition of lanthanides was successfully realized in second-generation ILs. The diffusion coefficients of Ln(III) ions in these ILs are typically smaller than those in haloaluminate ILs [*cf.* the data for Yb(III) and Sm(III) in Table 2] and fall in the range of 10^{-12} to 10^{-11} m^2 s^{-1} (with rare exceptions) depending on IL composition, lanthanide concentration and temperature. As a general comment one can also mention that the assignment of voltammetric features to reduction of lanthanides to Ln(0) is based on cyclic voltammetry and some *ex situ* microscopic and spectroscopic characterization. At the same time, the electroreduction can be a multistage process with possibility of competitive chemical side reactions, such as Ln(II) disproportionation and Ln(0) oxidation, as well as IL degradation with inclusion of degradation products into deposits. Additional *in situ* studies of lanthanide deposition in IL are highly required. Note that the electroreduction of lanthanides to metallic state was shown to be irreversible in most of the studies. The reversibility of the one-electron reduction of Ln(III) to Ln(II) seems to depend on the lanthanide itself, solution composition and temperature. Possible reasons for irreversibility of this process can be the disproportionation of Ln(II) (reaction 8) as well as the formation of a film that blocks the electrode surface and hinders the electrochemical reaction.

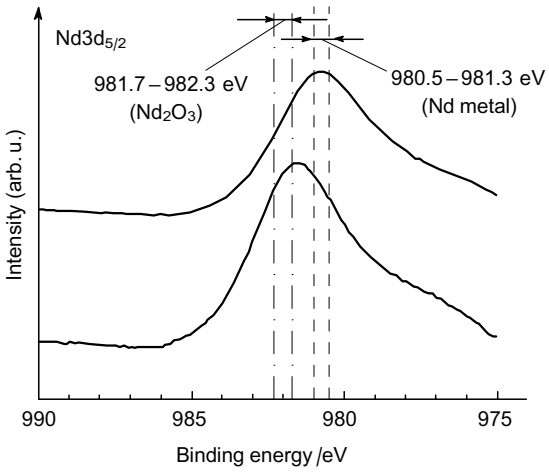


Figure 6. XPS spectra for $Nd3d_{5/2}$ region of electrodeposits with different depths: (*a*) top surface (981.5 eV) and (*b*) middle surface at 0.70 μm (980.5 eV). The dashed lines represent the range of the peak positions for metal and oxide forms of Nd. Reprinted with permission from Ref. 145.

4. Electrochemical co-deposition of lanthanide-based alloys from ionic liquids

The electrochemical deposition of lanthanide–transition metal (Ln-TM) alloys has gained significant attention, as these materials can have excellent magnetic, optical and electrical properties. The SmCo alloys, *e.g.*, have a high Curie temperature (excellent thermal magnetic stability), magnetic anisotropy and relatively high saturation magnetization and find important applications in microelectronic mechanical systems and high-density recording media,[152–154] Neodymium-based permanent magnets are commonly used in high-tech products such as electric vehicles and many electric devices,[155] GdCo alloy is reported to exhibit perpendicular magnetic anisotropy and can be used as a storage layer in magneto-optical storage media,[156] LnNi alloys can be applied as HER catalysts and as functional materials for hydrogen storage.[157,158] In addition, by co-deposition of lanthanides with other metals, novel catalytic materials can be obtained for electrochemical conversion of CO_2 to value-added products.[159] It is known that transition metals, such as Ag, Au, Cu, Zn, Sn, *etc.*, exhibit electrocatalytic properties in the electroreduction of CO_2. Besides, extensive studies are being conducted on combinations of various metals to change the adsorption energy of intermediates in the CO_2 reduction to achieve deeper reduction of CO_2 (for example, to methanol) and/or change the reaction pathway (*e.g.* to promote the formation of a carbon–carbon bond) and thereby increase the yield of certain products (ethanol, ethylene, *etc.*). It has been shown that Ce or CeOx both in contact with other metals (Ag, Au)[160] and in the absence of such a contact[161] can significantly accelerate the electrochemical reduction of CO_2 and affect the distribution of reaction products.

Several studies have demonstrated the electrodeposition of Ln-TM alloys in organic ionic systems. It was shown that the electroreduction of TM (having a more positive standard electrochemical potential than lanthanides) led to induced co-deposition of a lanthanide by a strong shift of its deposition potential to more positive values. This fact greatly simplifies the problem, since the deposition of pure

lanthanides requires a thorough search for a suitable ionic system that meets many requirements: solubility of the initial lanthanide salt, electrochemical stability of the solvent at high negative potentials, acceptable solution viscosity, *etc*. This induced electrochemical co-deposition was previously observed during the deposition of various alloys in aqueous solutions: *e.g*. CoRu,[162] ReNi,[163] WCo.[164] The electrodeposition of lanthanides and Fe-group elements (Fe, Ni, Co) in the form of films from aqueous solutions was also reported.[10,165–170] Different mechanisms were proposed to describe the induced co-deposition process. In particular, the induced co-deposition was explained by the influence of co-adsorbed hydrogen or TM adatoms[171,172] or the formation of complexes in solution, for example, between tungstate and a TM ion that were the reduced species.[173]

Recently, a theoretical model was proposed that described the co-deposition of Ln-TM alloys from organic ionic systems[174] at the example of [EMIm][DCA] containing $NdCl_3$ and $FeCl_2$ salts. The authors suggested that initially the Fe^{2+} ions were reduced to an intermediate species in the activated state Fe*, which, in turn, catalyzes the reduction of Nd(III) to Nd(0). In this study, the CV recorded in a 0.1 M $NdCl_3$ + [EMIM][DCA] solution displayed no voltammetric response corresponding to Nd(III) → Nd(0) reduction (curve *2* in Fig. 7), while the deposition of Fe was obviously observed in the 0.03 M $FeCl_2$ + [EMIM][DCA] solution (curve *3* in Fig. 7). When both salts were present in the IL, the cathodic peak current density increased significantly (curve *4* in Fig. 7), indicating the co-deposition of Fe and Nd. Thereby the onset of Nd deposition was shifted at least by 200 mV towards less negative potentials.

Amorphous NdFe films with a granular morphology were deposited using the galvanostatic pulsed-current technique.[174] Changing the concentration ratio of $NdCl_3$ and $FeCl_2$ in the solution allowed the tuning of the Nd content in the deposit in the range of ~6 at.% to 23 at.%. The estimated current efficiency during pulsed deposition was

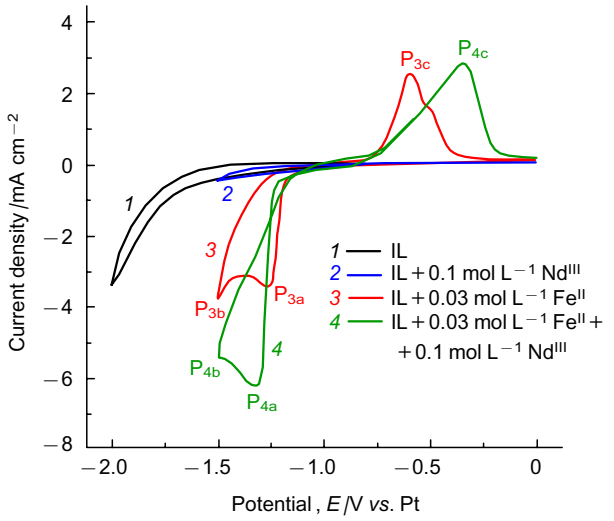


Figure 7. Cyclic voltammograms of a Pt electrode in (*1*) [EMIM][DCA], (*2*) 0.1 M $NdCl_3$ in [EMIM][DCA], (*3*) 0.03 M $FeCl_2$ in [EMIM][DCA] and (*4*) 0.03 M $FeCl_2$ + 0.1 M $NdCl_3$ in [EMIM][DCA], recorded at 383 K and ascanrate of 40 mV s^{-1}. Reprinted with permission from Ref. 174.

~70%, suggesting the competitive process of IL degradation. The analysis of the deposit cross-section by high-angle annular dark-field scanning transmission electron microscopy (TEM) and electron-energy-loss spectroscopy showed the existence of the initially deposited 3 nm-thick layer with its composition differing significantly from that of the bulk deposit: no Nd was detected, and the Fe content was higher in this thin layer than in the bulk. These observations supported the proposed model of induced Nd co-deposition,[174] showing that Fe was reduced first and then catalyzed the subsequent reduction of Nd(III).

Another dicyanamide IL, [BMP][DCA], was employed for the co-deposition of LaNi alloy at 333 K.[157] This IL showed better stability towards cathodic degradation than [EMIM][DCA].[175] The voltammetric responses, corresponding to La and Ni deposition, were observed in single-component solutions, 0.05 M $LaCl_3$ and 0.05 M $NiCl_2$ solutions in [BMP][DCA], respectively. Co-deposition of LaNi alloy was confirmed in the binary system (0.05 M $NiCl_2$ + 0.05 M $LaCl_3$). However, the onset of La deposition was not significantly shifted to more positive potentials upon co-deposition with Ni. The shift was within 100 mV, suggesting less effective induction of La co-deposition as compared to the Nd–Fe system in [EMIm][DCA].[174] Apparently, the induced co-deposition depends on the composition of the solution and the nature of Ln and TM. Furthermore, Gao *et al.*[157] reported the formation of amorphous granular deposits of LaNi alloys with 1 at.% to 8 at.% La depending on the applied potential. These LaNi deposits were tested in HER in an aqueous alkaline medium and exhibited rather a notable activity, which compared favourably with most other Ln–Ni HER catalysts, obtained by smelting.

Interesting results were reported by Manjum *et al.*,[176] who studied the co-deposition of SmCo alloy in [BMP][TFSI] at 298 K. The cyclic voltammogram of a GC electrode recorded in 5 mM $Sm(TFSI)_3$ displayed the redox peaks ascribed to the quasireversible Sm(III) ⇆ Sm(II) process. In the presence of 30 mM $Co(TFSI)_2$ and at the cathodic polarization of a working electrode (at potentials, where the Co(II) electrochemical reduction is insignificant, but the reduction of Sm(III) to Sm(II) is intensive), the authors observed the formation of nanoparticles both on the electrode surface and in the electrolyte solution. The SEM image demonstrates the granular deposit on the GC electrode (Fig. 8 *a*). Further, the deposit from the GC electrode was collected on a grid and examined by TEM (Fig. 8 *b*). The TEM image indicated clear lattice fringes in the nanoparticles, implying that the nanoparticles were crystalline. The crystallinity of the nanoparticles was further supported by EDX and XPS analyses, and the composition of $SmCo_7$ was proposed. Furthermore, TEM analyses showed that the nanoparticles found in the electrolyte solution were identical to the nanoparticles on the electrode surface (Fig. 8 *c*). The formation of $SmCo_7$ nanoparticles was explained by the fact that Sm(II) ions acted as both a reducing agent for Co(II) and a source of Sm(0) according to the reactions:

$$2\,Sm(II) + Co(II) \rightarrow 2Sm(III) + Co(0) \quad (18)$$

$$3\,Sm(II) + 7Co(0) \rightarrow 2\,Sm(III) + SmCo_7 \quad (19)$$

As argued by Manjum *et al.*,[176] the disproportionation reaction (8) of Sm(II) with the formation of Sm(III) and Sm(0) in the absence of Co(II) ions was insignificant at

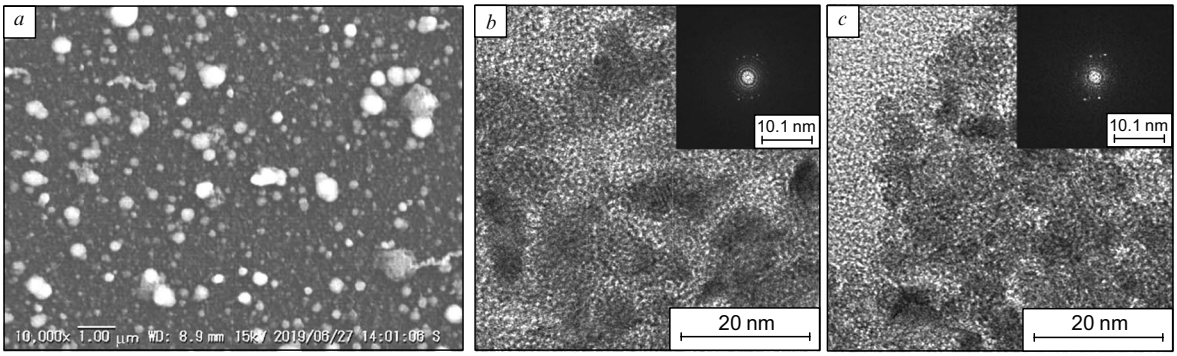


Figure 8. (*a*) SEM and (*b*) TEM images of the deposits obtained on a GC electrode after potentiostatic cathodic reduction at −1.6 V in [BMP][TFSI] containing 30 mM $Co(TFSI)_2$ and 5 mM $Sm(TFSI)_3$. Temperature: 298 K. Electric charge: 1.2 C. (*c*) TEM image of the nanoparticles dispersed in [BMP][TFSI] after potentiostatic cathodic reduction on a GC electrode. Reprinted with permission from Ref. 176.

298 K. This statement agrees with the previous reports, where the disproportionation of Sm(II) was observed at elevated temperatures,[81,87,88] while the stability of Sm(II) in [BMP][TFSI] was shown to increase at room temperature.[82,96] Nevertheless, the formation of SmCo nanoparticles on the electrode and in the solution and the proposed hypothesis should be further examined.

In the earlier paper, Ispas *et al.*[177] reported on the deposition of Sm and Co on a gold electrode from 0.05 M $Sm(TFSI)_3$ + 0.05 M $Co(TFSI)_2$ in [BMP][TFSI] and did not observe any formation of nanoparticles both at room temperature and at 393 K. The obtained SmCo deposits were proposed to be formed upon electrochemical reduction of Sm and Co.[177] Moreover, SEM/EDX analyses demonstrated a non-uniform distribution of Sm and Co in the deposited film over the electrode surface with Sm- or Co-rich regions. The latter phenomenon was explained by non-uniform current distribution on the working electrode surface. However, taking into account the ability of Sm(II) ions to disproportionate to Sm(III) and Sm(0) [reaction (8)][81,82,87,88,96] especially at elevated temperature, one can suggest that the disproportionation reaction can take place [at least, in parallel to the electrochemical Sm(0) formation] and may be one of the reasons for non-uniform Sm distribution in the deposit.

In summary, the induced electrochemical co-deposition of Ln and TM from ILs has been demonstrated at the example of NdFe, SmCo and LaNi, and obviously this approach hold promise and opens additional opportunities for formation of various lanthanide-containing materials using electrochemical methods.

5. Electrodeposition of lanthanides and lanthanide-based alloys from deep eutectic solvents

The major application of DESs can be metal extraction and deposition.[39] Despite the growing research interest in the electrodeposition of various metals in DESs (examples are deposition of Ag,[178,179] Ni,[180] ZnSn alloy,[181] NiCo alloy[182]), there are few publications on lanthanide deposition in such systems. Especially, the electrochemical formation of pure lanthanide deposits from DESs has not been progressed much. Apparently, the reduction of Ln(III) species occurs at the potentials, where the reductive degradation of DES components is already rather intensive. However, as shown further, the electrochemical co-deposition of Ln-TM alloys was successfully realized in different types of DESs.

Several studies have demonstrated the electrodeposition of Ln-TM alloys in urea-based melts at elevated temperatures (typically 343 to 403 K): NdFe from $NdCl_3 - FeCl_2 -$ acetamide $-$ urea $-$ NaBr $-$ KBr;[183] SmCo from $SmCl_3 - CoCl_2 -$ acetamide $-$ urea $-$ NaBr;[184] LaCo from $LaCl_3 - CoSO_4 -$ urea $-$ NaBr;[185] SmFe, GdCo and LaNi from urea $-$ acetamide $-$ NaBr $-$ KBr $- LnCl_3 - TMCl_2$ (where Ln and TM are the respective lanthanide and transition metal).[186] Pure lanthanide deposits cannot be obtained from this melt in the absence of the respective TM ions at least at potentials more positive than that of the reductive degradation of the melt. Liu *et al.*[184] studied co-deposition of SmCo and suggested that the induced co-deposition in this melt was related to the formation of a polynuclear complex containing Co(II) and Sm(III) as electroactive intermediates. Li *et al.*[186] compared the different dependences of lanthanide content in SmFe, GdCo and LaNi alloy deposits on the deposition potential and concluded that the possibility and efficiency of induced lanthanide co-deposition were determined by the electronegativity difference between Ln and TM elements.

Reline (choline chloride – urea mixture in a molar ratio of 1 : 2), the most archetypal DES, was employed for the electrodeposition of lanthanides and lanthanide-based alloys in a few studies. Liu *et al.*[150] reported the induced electrochemical co-deposition of NdCo alloy from 0.029 M $NdCl_3$ + 0.039 M $CoCl_2$ in reline at 373 K. The authors indicated that the deposition of Nd from reline containing only a Nd(III) salt was impossible. The NdCo alloy deposits with the maximum Nd content of 3.74 wt.% were obtained in a potentiostatic mode in the presence of both salts.[150] The electrodeposition of amorphous ternary PrMgCo alloy films from reline at 353 K was recently reported by Li *et al.*[187] In this study, the Pr content in the ternary alloy deposit was up to 13.2 wt.%; however, the oxidation states of Co, Mg and Pr were not examined.

The possibility of electrodeposition of Sm and SmCo alloy from reline at 343 K was demonstrated by Gómez *et al.*[188] Cyclic voltammograms of a GC electrode recorded in reline + 0.045 M $Sm(NO_3)_3$ revealed two reduction waves. In the first reduction region (low overpotentials), the reduction process was hindered probably due to the formation of a passivating film. At more negative potentials

($\leqslant -1.9$ V *vs* $Ag/AgCl_{3M\ NaCl}$, or ~ -2.3 V *vs* Fc/Fc^+), however, Sm deposition was accelerated. According to SEM, the deposit obtained at -1.9 V was rather flat. The addition of 0.018 M $CoCl_2$ to the Sm solution (the Sm : Co molar ratio was 4 : 1) led to induced Sm co-deposition: the potential onset of Sm deposition was slightly shifted to more positive values. Compact granular SmCo deposits were obtained in the course of potentiostatic deposition on GC as well as on metallic substrates with a Sm content of up to 80 wt.%.[188] Notably, a nucleation loop was observed in cyclic voltammograms for Co deposition in reline, whereas the nucleation loop was not present in the case of Sm and SmCo deposition, indicating different nucleation and growth mechanisms.[188, 189] Uniform SmCo deposits of 3 – 5 μm thickness containing 50 wt.% Sm were obtained in the 0.040 M Sm(III) + 0.045 M Co(II) solution in reline.[189] Moreover, Gómez *et al.* also achieved the electrodeposition of well-defined Sm – Co nanowires using a porous alumina template.[189, 190]

Chen *et al.*[152] performed electrodeposition of SmCo alloy nanowires from $SmCl_3 - CoCl_2 -$ [EMIm][Cl] melts of different compositions at elevated temperature (363 and 393 K) without any template.[152] The selected area electron diffraction and high-resolution TEM analyses showed a mainly amorphous state of SmCo nanowires. The Sm content in the nanowires was estimated from EDX spectra to range from 3 mol.% to 37 mol.% depending on the ionic melt composition.[152]

Another DES, ethaline [choline chloride/ethylene glycol (EG) mixture in a molar ratio 1 : 2], was also employed for electrochemical co-deposition of Ln-TM alloys. For example, CeNi alloy deposits were obtained from ethaline containing $NiCl_2$, $CeCl_3$, NH_4Cl and H_3BO_3.[191] Recently, Panzeri *et al.*[153, 192] studied the electrochemical deposition of SmCo in ethaline at 343 K. Rather flat (but with cracks) SmCo alloy deposits with a Sm content of about 20 wt.% were obtained in 0.040 M $CoCl_2$ + 0.040 M $SmCl_3$ ethaline solutions in the presence of glycine. This SmCo composition is close to the optimal one, corresponding to the Sm_2Co_{17} phase that exhibits the best magnetic properties. The addition of glycine as a complexing agent was stated by the authors [153, 192] to affect the growth kinetics and morphology of the deposit and to lead to an increase in Sm content. However, it is worth noting that Co(II) and Sm(III) were introduced into ethaline as chloride hexahydrates. Also with account for high hygroscopicity of choline chloride, the amount of water in the electrolyte system may be enough to affect the kinetics and morphology of the deposits because of HER. Moreover, the potential window of ethaline stability is rather limited by the reduction of EG, and the SmCo deposition process overlaps with the reduction of EG and residual water. The authors also pointed out the presence of oxygen in the deposits,[192] which can be due to the chemical oxidation of Sm(0) in the presence of water.

A eutectic-based ionic system, [EMIm][Cl]-EG (1 : 2 ratio), was employed as a medium for electrochemical deposition of LaNi alloys.[193] The deposition was studied on GC and Cu electrodes in a 0.1 M $NiCl_2$ + 0.2 M $LaCl_3$ solution at elevated temperature (353 – 373 K). The reductive decomposition of [EMIm][Cl]-EG (1 : 2) was found to start at -1.67 V *vs* Ag quasi-reference electrode (Ag wire). The La(III) reduction from the solution containing only the La(III) salt was not detected in the potential region prior to DES degradation. In the solution containing both components [La(III) and Ni(II)], two cathodic waves were observed, at $\sim$-0.7 V (Ni reduction) and ~ -1.3 V (La reduction), indicating induced co-deposition of La. Potentiostatic current transient measurements showed the instantaneous nucleation and three-dimensional diffusion-controlled growth. The bulk deposits obtained on a Cu substrate in a galvanostatic mode had porous granular structure. The La content in the deposits grew (up to $\sim$9.5 at.%) with increasing temperature and applied current density. The XRD patterns measured for deposits with different La content suggested the formation of LaNi alloy; the deposits displayed crystalline structure at <4 at.% La and were completely amorphous at 9.5 at.%.[193] The authors also claimed that the deposits fell off from the substrate when a higher cathodic current density (10 A cm^{-2}) was applied in the attempt to obtain higher La content.

DESs of the fourth type (metal salt + molecular component) were prepared by mixing Ce, Nd and Pr nitrate hydrates with urea (1 : 3.5 molar ratio).[66] The glass transition temperature of these DESs was found to be 215 K, which is a significant eutectic depression [the melting point of urea is 406 K, and *e.g.* that of $Ce(NO_3)_3 \cdot 6H_2O$ is 369 K]. These DESs also have relatively moderate viscosity (much lower than the viscosity of reline): *e.g.* 168 mPa s for the Ce-based DES (see Table 1). Hammond *et al.*[66] used neutron and X-ray scattering and atomistic modelling to investigate the structure of lanthanide-based DESs. The structure was proposed to be similar to that of chlorometallate ILs, consisting of a variety of polyanions and polycations. Although neither electrochemical properties nor conductivity of these systems were reported, one could expect that lanthanide deposition from this type of DESs is possible in principle.

6. Solubility and viscosity issues: challenges and prospects

Among various issues that affect the electrodeposition process, the solubility of metal salts in a liquid medium is of primary importance since a high concentration of a metal salt in deposition solutions is a prerequisite for industrial implementation. The problem of lanthanide salt solubility and complex formation in various types of ILs is addressed in a few recent reviews,[29, 194, 195] although quantitative data on the solubility of lanthanide salts in ILs are scarce. In general, the solubility of ionic inorganic compounds in ILs is often very low. It was reported that chlorides of lanthanides and other transition metals were poorly soluble in the conventional imidazolium ILs.[196, 197] This problem arises from the low solvating power of ILs with weakly coordinating anions like $[BF_4]^-$, $[PF_6]^-$ or $[TFSI]^-$.[195, 198, 199] On the contrary, haloaluminate ILs are good solvents for a number of transition metal salts, including lanthanide salts;[73] however, they are moisture-sensitive and Al is usually co-deposited with lanthanides.[73, 74]

Good solubility of lanthanides in [TFSI]-based ILs can be achieved by the introduction of $Ln(TFSI)_3$ salts. For instance, the solubility of $Nd(TFSI)_3$ and $Dy(TFSI)_3$ reached $\sim$1.5 M in $[P_{2,2,2,5}][TFSI]$ at an elevated temperature of $\sim$373 K[105] and at least 0.5 M in the same IL at room temperature.[121] Although $Ln(TFSI)_3$ can be easily dissolved in TFSI-based ILs (see [200]) and look promising for lanthanide electroplating, a very high cost and a complicated synthesis procedure interfere with their application. Moreover, $Ln(TFSI)_3$/[cation][TFSI] electrolyte solutions

would be economically inefficient for the lanthanide deposition due to anodic oxidation of $[TFSI]^-$ anions as a counter electrode reaction. To overcome the problem of the anodic reaction, lanthanides can be deposited from lanthanide chloride solutions, since the anodic reaction is chlorine evolution. However, chloride salts are poorly solube in most of the second-generation ILs. A promising exception was found to be [DCA]-based ILs, providing an appreciable solubilizing ability for $LnCl_3$ salts.[63,133] Better solubility of inorganic salts in the [DCA]-based ILs can be due to donor ligand properties of $[DCA]^-$ anions.[62,201] Choline-chloride DESs demonstrate a good solubilizing ability for metal salts (including chlorides) as well as for oxides[39,202–204] and can be used for leaching and electrodeposition of lanthanides.

The so-called task-specific ILs can be designed to exhibit excellent ability to solubilize metal salts.[202] Recently, to increase the solubilizing ability of ILs towards lanthanide salts/oxides, imidazolium-, pyridinium-, pyrrolidinium-, piperidinium-, morpholinium- and quaternary ammonium-[TFSI] ILs were functionalized with a carboxyl group.[198,205,206] Such functionalized ILs are useful for selective dissolution of metal oxides and hydroxides, producing metal-carboxylate-functionalized ILs. However, the melting points of these functionalized ILs are above room temperature (but still <373 K).[83] Various types of ionic melts with lanthanide-containing anions (based on lanthanide halides, nitrates or thiocyanates, β-diketonate compounds of lanthanides) are summarized in the review.[83] Among these ionic melts, low melting points (below room temperature) were observed for imidazolium ILs with lanthanide thiocyanate anions $[Ln(NCS)_x(H_2O)_y]^{3-x}$ (where $x = 6-8$; $y = 0-2$; $x + y < 10$; Ln = Y, La–Yb)[207] and for phosphonium ILs with the lanthanide chloride anion $[P_{6,6,6,14}]_3[LnCl_6]$.[138] The lanthanide-thiocyanate ILs have, however, low thermal stability and start decomposing at rather moderate temperatures (below 350 K).[207] The electrochemical properties of these ILs were studied in a few articles, where only quasireversible reduction of Ln(III) to Ln(II) was demonstrated.[138,208] Although electrochemical deposition from lanthanide-containing ILs has not been studied as yet, this approach to obtaining an ionic system with an extremely high lanthanide concentration is very attractive. The use of *neutral ligands*, which can form complexes with Ln(III), to prepare NLILs for lanthanide deposition is another promising approach due to the potentially high solubilizing ability of NLILs.[143–146]

Solvent viscosity is another important property affecting mass transport, reaction kinetics, electrical conductivity and ease of handling. Low-viscosity ILs and DESs are preferable for the electrodeposition.[209,210] Among non-halometallate ILs, employed to investigate electrochemical properties of lanthanides, ILs with the $[DCA]^-$ anion exhibit the lowest viscosity (see Table 1) comparable to the viscosity of EG. Ionic liquids with the $[DCA]^-$ anions and ILs with other cyano-based anions, such as tricyanomethanide ($[TCM]^-$) and tetracyanoborate ($[TCB]^-$) showing relatively low viscosity and good solubilizing ability,[62] can be a promising medium for the electrodeposition of metals. However, the studies on lanthanide electrodeposition from these ILs are scarce (only from [DCA]-based ILs[12,133,135,157,174]). It is worthy of note that the ILs with imidazolium cations (especially with $[EMIm]^+$, see Table 1) show lower viscosity than ILs with other common cations ($[BMP]^+$, $[N_{1,1,1,4}]^+$, $[P_{2,2,2,5}]^+$). However, imidazolium cations demonstrate lower stability at negative potentials (the cathodic limit of IL stability is mostly dependent on the cation[211]), and therefore the attempts to deposit highly reactive metals in imidazolium ILs often resulted in reductive degradation of imidazolium cations.[103,145,209,211,212] On the other hand, the ILs with more stable cations such as pyrrolidinium, ammonium and phosphonium allow lanthanide deposition. Recently, Strassner's group introduced a new class of imidazolium-based ILs — the so-called tunable aryl alkyl ILs with the $[TFSI]^-$ and $[DCA]^-$ anions.[213] These ILs demonstrated significant electrochemical stability (the electrochemical window reached 7 V), which is very beneficial for the electrodeposition of lanthanides. Although the viscosity of these ILs is quite high at room temperature (a few hundreds of mPa s at 293 K), it drops below 50 mPa s as temperature increases to 343 K.[213]

The viscosity of solvents typically increases with decreasing temperature. More importantly, the viscosity of the system may significantly rise with increasing lanthanide salt concentration in the ILs as nicely demonstrated for the $Dy(TFSI)_3/[P_{2,2,2,5}][TFSI]$ system (Fig. 9).[104] In this example, the viscosity increased from ~80 to ~350 mPa s at 303 K for the 0.075 M Dy(III) and 0.5 M Dy(III) concentrations, respectively. In another example, the viscosity of $[P_{2,2,2,5}][TFSI]$ was reported to increase by approximately an order of magnitude upon dissolution of 0.5 M $Nd(TFSI)_3$.[121] Since the diffusion coefficient of solutes is inversely related to viscosity (according to the Stokes–Einstein equation), the diffusion coefficient of Dy(III) inversely depends on temperature and also changes (decreases) accordingly with increasing salt concentration (Fig. 9, Table 2). It was also shown that the conductivity varies inversely with the IL viscosity.[121,214] Thus, the rate of diffusion-controlled electrodeposition can be improved by a proper choice of the IL or DES composition, the concentration of lanthanide ions and temperature.

A promising approach comprises the use of mixtures of ILs and molecular solvents (MSs). The development of such mixtures may allow fine tuning of the physicochemical properties of electrolyte systems.[215] Particularly, the viscosity of ILs can be lowered by a proper choice of the mixture concentration.[216,217] The effect is very pronounced for

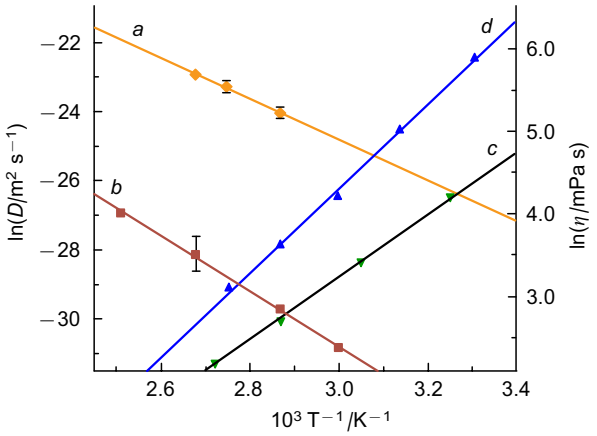


Figure 9. Arrhenius plots of (*a*, *b*) diffusion coefficients of Dy(III) and (*c*, *d*) viscosity values for (*a*, *c*) 0.075 M Dy(III) and (*b*, *d*) 0.5 M Dy(III) in $[P_{2,2,2,5}][TFSI]$. Reprinted with permission from Ref. 104.

highly viscous ILs. As an example, the viscosity of 1-octyl-3-methylimidazolium chloride, [OMIm][Cl], equal to 7340 mPa s at 303 K, decreases by a factor of nearly 10 in the mixture with DMFA in a molar ratio of 2.8 : 1 and by the factor of 158 for the ratio of 1 : 1. Besides lowering viscosity, IL + MS mixtures may provide low volatility,[218] which eliminates hazards and toxicity of these electrolyte systems as compared to conventional industrial solvents. The dilution of DESs by a low-viscosity solvent can also lead to a significant decrease in the viscosity.[219]

7. Conclusion

Analysis of publications shows that the electrodeposition of lanthanides from different ionic systems such as ILs, DESs and other low-melting mixtures is possible in principle and promising. However, the electrochemical formation of lanthanide metal deposits is a non-trivial process and hitherto little studied. The irreversibility of Ln(III) to Ln(0) reduction, the inclusion of IL or DES decomposition products and/or partial oxidation of lanthanide deposits in the presence of residual or added water, the formation of passivating films, the formation of divalent lanthanide species and their possible disproportionation complicate the investigation of the electrodeposition process, especially of the initial stages of deposition, *i.e.* nucleation and crystallite growth. It is obvious that the use of only electrochemical techniques is insufficient for studying lanthanide electrodeposition. The combination of electrochemistry with different types of spectroscopic and microscopic analyses is essential to examine the morphology, elemental composition, oxidation state, alloying and crystallinity of the obtained deposits. The study of lanthanide nucleation and growth will also benefit from the combination of electrochemical measurements and scanning probe microscopy (SPM). The *in situ* visualization of the initial stages of electrodeposition by SPM with up to atomic-scale resolution may provide important information on the nucleation/growth mechanisms and on the effect of the substrate material and surface structure.[175, 178] Furthermore, the fundamental aspects such as the speciation and mass transport of lanthanide ions in ILs, electrode/IL interface structure, adsorption of ionic species on the electrode and deposit surface have to be systematically investigated. The full understanding of the lanthanide electrodeposition process in ILs and low-melting mixtures is an important step towards the efficient recycling of lanthanides and electrochemical formation of lanthanide-based functional materials. The further search for and design of new ionic systems, including lanthanide-containing ILs and DESs, can certainly make lanthanide electrodeposition more efficient and economically feasible.

The work was supported by the Russian Foundation for Basic Research (Project Nos 20-53-10007 and 20-03-00612) and by the Ministry of Science and Higher Education of the Russian Federation.

References

1. V.Zepf. In *Rare earths industry*. (Eds I.Borges De Lima, W.Leal Filho). (Boston: Elsevier, 2016). P. 3
2. S.V.Eliseeva, J.-C.G.Bünzli. *New J. Chem.*, **35**, 1165 (2011)
3. *Study on the review of the list of Critical Raw Materials: Executive Summary*; https://ec.europa.eu/docsroom/documents/25421/attachments/1/translations/en/renditions/native 2017 (Last accessed 02.11.2020)
4. S.M.Hayes, E.A.McCullough. *Resour. Policy*, **59**, 192 (2018)
5. K.Binnemans, P.T.Jones. *J. Sustain. Metall.*, **1**, 29 (2015)
6. F.Habashi. *Can. Metall. Q.*, **52**, 224 (2013)
7. P.Davris, E.Balomenos, M.Taxiarchou, D.Panias, I.Paspaliaris. *BHM Berg- und Hüttenmännische Monatshefte*, **162**, 245 (2017)
8. D.R.Lide. *CRC Handbook of Chemistry and Physics*. 90th Edition. (Boca Raton, FL: CRC Press, 2009). 2804 p.
9. T.Moeller. *The Chemistry of the Lanthanides*. (Great Britain: Pergamon, 1973). P. 1
10. J. Zhang, P.Evans, G.Zangari. *J. Magn. Magn. Mater.*, **283**, 89 (2004)
11. E.Bourbos, I.Giannopoulou, A.Karantonis, I.Paspaliaris, D.Panias. In *Rare Earths Industry*. (Eds I.Borges De Lima, W.Leal Filho). (Boston: Elsevier, 2016). P. 199
12. L.J.Small, J.M.Sears, T.N.Lambert, T.J.Boyle, R.F.Hess. *RSC Adv.*, **6**, 89564 (2016)
13. V.Smolenski, A.Novoselova, A.Osipenko, C.Caravaca, G.de Córdoba. *Electrochim. Acta*, **54**, 382 (2008)
14. V.Smolenski, A.Novoselova, A.Osipenko, M.Kormilitsyn. *J. Electroanal. Chem.*, **633**, 291 (2009)
15. A.Saïla, M.Gibilaro, L. Massot, P.Chamelot, P.Taxil, A.M.Affoune. *J. Electroanal. Chem.*, **642**, 150 (2010)
16. Y.Castrillejo, M.R.Bermejo, A.I.Barrado, R.Pardo, E.Barrado, A.M.Martínez. *Electrochim. Acta*, **50**, 2047 (2005)
17. H.Konishi, H.Hua, H.Ono, Y.Koizumi, T.Oishi, T.Nohira. *ECS Trans.*, **86**, 321 (2018)
18. D.Shen, R.Akolkar. *J.Electrochem. Soc.*, **164**, H5292 (2017)
19. K.Liu, Y.-L.Liu, L.-Y.Yuan, X.-L.Zhao, H.He, G.-A.Ye, Z.-F.Chai, W.-Q.Shi. *Electrochim. Acta*, **116**, 434 (2014)
20. K.Yasuda, S.Kobayashi, T.Nohira, R.Hagiwara. *Electrochim. Acta*, **106**, 293 (2013)
21. A.Abbasalizadeh, A.Malfliet, S.Seetharaman, J.Sietsma, Y.Yang. *J. Sustain. Metall.*, **3**, 627 (2017)
22. Y.Gu, J.Liu, S.Qu, Y.Deng, X. Han, W.Hu, C.Zhong. *J. Alloys Compd.*, **690**, 228 (2017)
23. P.Liu, Q.Yang, Y.Tong, Y.Yang. *Electrochim. Acta*, **45**, 2147 (2000)
24. G.-R.Li, G.-K.Liu, Y.-X.Tong. *Electrochem. Commun.*, **6**, 441 (2004)
25. M.Z.An, J.L.Wang, D.Z.Sun. *J. Appl. Electrochem.*, **31**, 891 (2001)
26. S.Yuichi, I.Hiroshi, K.Koichi, A.Yuki. *Chem Lett.*, **19**, 1471 (1990)
27. J.Lodermeyer, M.Multerer, M.Zistler, S.Jordan, H.J.Gores, W.Kipferl, E.Diaconu, M.Sperl, G.Bayreuther. *J. Electrochem. Soc.*, **153**, C242 (2006)
28. E.Bourbos, A.Karantonis, L.Sygellou, I.Paspaliaris, D.Panias. *Metals*, **8**, 803 (2018)
29. K.Binnemans. *Chem. Rev.*, **107**, 2592 (2007)
30. S.Kazemiabnavi, Z.Zhang, K.Thornton, S.Banerjee. *J. Phys. Chem. B*, **120**, 5691 (2016)
31. M.V.Fedorov, A.A.Kornyshev. *Chem. Rev.*, **114**, 2978 (2014)
32. L.A.Aslanov, M.A.Zakharov, N.L.Abramycheva. *Ionic Liquids as Solvents. (Ionic Liquids as Solvents)*. (Moscow: Moscow University Press, 2005). 272 p.
33. A.P.Abbott, F.Endres, D.R.Macfarlane. In *Electrodeposition from Ionic Liquids*. (Eds F.Endres, A.Abbott, D.MacFarlane). (Weinheim: Wiley-VCH, 2017). P. 1
34. T.Torimoto, T.Tsuda, K.-i.Okazaki, S.Kuwabata. *Adv. Mater.*, **22**, 1196 (2010)
35. Q.Zhang, Q.Wang, S.Zhang, X.Lu, X.Zhang. *ChemPhysChem*, **17**, 335 (2016)
36. F.Liu, Y.Deng, X.Han, W.Hu, C.Zhong. *J. Alloys Compd.*, **654**, 163 (2016)
37. P.Sebastián, V.Climent, J.M.Feliu, E.Gómez. In *Encyclopedia of Interfacial Chemistry: Surface Science and Electrochemistry*. (Ed. K.Wandelt). (Elsevier, 2018). P. 690
38. O.K.Lebedeva, D.Y.Kul'tin, L.M.Kustov, S.F.Dunaev. *Ros. Khim. Zh. (Green Chem.)*, **48** (6), 59 (2004)

39. E.L.Smith, A.P.Abbott, K.S.Ryder. *Chem. Rev.*, **114**, 11060 (2014)
40. T.Beyersdorff, T.J.S.Schubert, U. Welz-Biermann, W.Pitner, A.P.Abbott, K.J.McKenzie, K.S.Ryder. In *Electrodeposition from Ionic Liquids*. (Eds F.Endres, A.Abbott, D.MacFarlane). (Weinheim: Wiley-VCH, 2017). P. 17
41. A.P.Abbott, A.A.Al-Barzinjy, P.D.Abbott, G.Frisch, R.C.Harris, J.Hartley, K.S.Ryder. *Phys. Chem. Chem. Phys.*, **16**, 9047 (2014)
42. B.Kudłak, K.Owczarek, J.Namieśnik. *Environ. Sci. Pollut. Res.*, **22**, 11975 (2015)
43. B.Gurkan, H.Squire, E.Pentzer. *J. Phys. Chem. Lett.*, **10**, 7956 (2019)
44. I.Juneidi, M.Hayyan, M.A.Hashim. *RSC Adv.*, **5**, 83636 (2015)
45. Z.Yang. In *Deep Eutectic Solvents: Synthesis, Properties, and Applications*. (Eds D.J.Ramón, G.Guillena). (Wiley-VCH, 2019). P. 43
46. Y.Zheng, Y.Zheng, Q.Wang, Z.Wang, D.Tian. *J. Chem. Eng. Data*, **62**, 4006 (2017)
47. W.Ochędzan-Siodłak, K.Dziubek, D.Siodłak. *J. Mol. Liq.*, **177**, 85 (2013)
48. C.Schreiner, S.Zugmann, R.Hartl, H.J.Gores. *J. Chem. Eng. Data*, **55**, 1784 (2010)
49. J.Jacquemin, P.Husson, A.A.H.Padua, V.Majer. *Green Chem.*, **8**, 172 (2006)
50. H.F.D.Almeida, J.N.Canongia Lopes, L.P.N.Rebelo, J.A.P.Coutinho, M.G.Freire, I.M.Marrucho. *J. Chem. Eng. Data*, **61**, 2828 (2016)
51. H.Tokuda, S.Tsuzuki, M.A.B.H.Susan, K.Hayamizu, M.Watanabe. *J. Phys. Chem. B*, **110**, 19593 (2006)
52. M.Biso, M.Mastragostino, M.Montanino, S.Passerini, F.Soavi. *Electrochim. Acta*, **53**, 7967 (2008)
53. M.Tariq, P.J.Carvalho, J.A.P.Coutinho, I.M.Marrucho, J.N.C.Lopes, L.P.N.Rebelo. *Fluid Phase Equilib.*, **301**, 22 (2011)
54. M.Vranes, S.Dozic, V.Djeric, S.Gadzuric. *J. Chem. Eng. Data*, **57**, 1072 (2012)
55. M.Dakkach, F.M.Gaciño, M.J.G.Guimarey, S.K.Mylona, X.Paredes, M.J.P.Comuñas, J.Fernández, M.J.Assael. *J. Chem. Thermodyn.*, **121**, 27 (2018)
56. S.Legeai, S.Diliberto, N.Stein, C.Boulanger, J.Estager, N.Papaiconomou, M.Draye. *Electrochem. Commun.*, **10**, 1661 (2008)
57. D.R.McFarlane, J.Sun, J.Golding, P.Meakin, M.Forsyth. *Electrochim. Acta*, **45**, 1271 (2000)
58. K.Tsunashima, M.Sugiya. *Electrochem. Commun.*, **9**, 2353 (2007)
59. C.M.S.S.Neves, P.J.Carvalho, M.G.Freire, J.A.P.Coutinho. *J. Chem. Thermodyn.*, **43**, 948 (2011)
60. R.Nagaishi, M.Arisaka, T.Kimura, Y.Kitatsuji. *J. Alloys Compd.*, **431**, 221 (2007)
61. N.Bucher, S.Hartung, M.Arkhipova, D.Yu, P.Kratzer, G.Maas, M.Srinivasan, H.E.Hoster. *RSC Adv.*, **4**, 1996 (2014)
62. D.R.MacFarlane, S.A.Forsyth, J.Golding, G.B.Deacon. *Green Chem.*, **4**, 444 (2002)
63. W.-L.Yuan, X.Yang, L.He, Y.Xue, S.Qin, G.-H.Tao. *Front. Chem.*, **6**, 59 (2018)
64. S.Bi, T.M.Koller, M.H.Rausch, P.Wasserscheid, A.P.Fröba. *Ind. Eng. Chem. Res.*, **54**, 3071 (2015)
65. C.D'Agostino, R.C.Harris, A.P.Abbott, L.F.Gladden, M.D.Mantle. *Phys. Chem. Chem. Phys.*, **13**, 21383 (2011)
66. O.S.Hammond, D.T.Bowron, K.J.Edler. *ACS Sustain. Chem. Eng.*, **7**, 4932 (2019)
67. J.P.Schoebrechts, B.P.Gilbert, G.Duyckaerts. *J. Electroan. Chem. Interfacial Electrochem.*, **145**, 127 (1983)
68. J.P.Schoebrechts, B.P.Gilbert, G.Duyckaerts. *J. Electroan. Chem. Interfacial Electrochem.*, **145**, 139 (1983)
69. C.K.JØrgensen. *Chem. Phys. Lett.*, **2**, 549 (1968)
70. L.J.Nugent, R.D.Baybarz, J.L.Burnett, J.L.Ryan. *J. Phys. Chem.*, **77**, 1528 (1973)
71. G.Duyckaerts, B.Gilbert. *Inorg. Nucl. Chem. Lett.*, **13**, 537 (1977)
72. B.Gilbert, V.Demarteau, G.Duyckaerts. *J. Electroan. Chem. Interfacial Electrochem.*, **89**, 123 (1978)
73. T.Tsuda, T.Nohira, Y.Ito. *Electrochim. Acta*, **46**, 1891 (2001)
74. T.Tsuda, T.Nohira, Y.Ito. *Electrochim. Acta*, **47**, 2817 (2002)
75. J.Fuller. *J. Electrochem. Soc.*, **143**, L145 (1996)
76. B.Zhang, Z.Shi, L.Shen, X.Liu, J.Xu, Z.Wang. *J. Solid State Electrochem.*, **23**, 1903 (2019)
77. W.-J.Gau, I.-W.Sun. *J. Electrochem. Soc.*, **143**, 914 (1996)
78. W.-J.Gau, I.-W.Sun. *J. Electrochem. Soc.*, **143**, 170 (1996)
79. A.Babai, S.Pitula, A.-V.Mudring. *Eur. J. Inorg. Chem.*, **2010**, 4933 (2010)
80. H.-Y.Hsu, C.-C.Yang. *Z. Naturforsch., B*, **58b**, 139 (2003)
81. Y.Pan, C.L.Hussey. *Inorg. Chem.*, **52**, 3241 (2013)
82. M.Yamagata, Y.Katayama, T.Miura. *J. Electrochem. Soc.*, **153**, E5 (2006)
83. D.Prodius, A.-V.Mudring. *Coord. Chem. Rev.*, **363**, 1 (2018)
84. N.Sánchez-Ramírez, B.D.Assresahegn, D.Bélanger, R.M.Torresi. *J. Chem. Eng. Data*, **62**, 3437 (2017)
85. C.Jagadeeswara Rao, K.A.Venkatesan, K.Nagarajan, T.G.Srinivasan, P.R.Vasudeva Rao. *Electrochim. Acta*, **54**, 4718 (2009)
86. G.Suppan, M.Ruehrig, A.Kanitz, H.J.Gores. *J. Electrochem. Soc.*, **162**, D382 (2015)
87. L.-H.Chou, W.E.Cleland, C.L.Hussey. *Inorg. Chem.*, **51**, 11450 (2012)
88. L.-H.Chou, C.L.Hussey. *Inorg. Chem.*, **53**, 5750 (2014)
89. K.Fukasawa, A.Uehara, T.Nagai, T.Fujii, H.Yamana. *J. Nucl. Mater.*, **414**, 265 (2011)
90. R.Hagiwara, M.Ito, Y.Ito. *Carbon*, **34**, 1591 (1996)
91. A.P.Abbott, G.Frisch, J.Hartley, W.O. Karim, K.S.Ryder. *Prog. Nat. Sci-Mater.*, **25**, 595 (2015)
92. D.R.MacFarlane, M.Forsyth, P.C.Howlett, J.M.Pringle, J.Sun, G.Annat, W.Neil, E.I.Izgorodina. *Acc. Chem. Res.*, **40**, 1165 (2007)
93. P.C.Howlett, N.Brack, A.F.Hollenkamp, M.Forsyth, D.R.MacFarlane. *J. Electrochem. Soc.*, **153**, A595 (2006)
94. E.B.Molodkina, M.R.Ehrenburg, P.Broekmann, A.V.Rudnev. *J. Electroanal. Chem.*, **860**, 113892 (2020)
95. E.Bourbos, I.Giannopoulou, A.Karantonis, I.Paspaliaris, D.Panias. *J. Sustain. Metall.*, **4**, 395 (2018)
96. M.Manjum, N.Tachikawa, N.Serizawa, Y.Katayama. *J. Electrochem. Soc.*, **166**, D483 (2019)
97. D.W.Hatchett, J.Droessler, J.M.Kinyanjui, B.Martinez, K.R.Czerwinski. *Electrochim. Acta*, **89**, 144 (2013)
98. J.M.Klein, E.Panichi, B.Gurkan. *Phys. Chem. Chem. Phys.*, **21**, 3712 (2019)
99. A.Saheb, J.Janata, M.Josowicz. *Electroanal.*, **18**, 405 (2006)
100. A.I.Bhatt, I.May, V.A.Volkovich, D.Collison, M.Helliwell, I.B.Polovov, R.G.Lewin. *Inorg. Chem.*, **44**, 4934 (2005)
101. V.A.Safonov, H.Habazaki, P.Glatzel, L.A.Fishgoit, O.A.Drozhzhin, S.Lafuerza, O.V.Safonova. *Appl. Surf. Sci.*, **427**, 566 (2018)
102. Y.M.Polukarov, V.A.Safonov, A.A.Edigaryan, L.N.Vykhodtseva. *Prot. Met.*, **37**, 447 (2001)
103. A.M.O'Mahony, D.S.Silvester, L.Aldous, C.Hardacre, R.G.Compton. *J. Chem. Eng. Data*, **53**, 2884 (2008)
104. A.Kurachi, M.Matsumiya, K.Tsunashima, S.Kodama. *J. Appl. Electrochem.*, **42**, 961 (2012)
105. R.Kazama, M.Matsumiya, N.Tsuda, K.Tsunashima. *Electrochim. Acta*, **113**, 269 (2013)
106. M.Matsumiya, M.Ishii, R.Kazama, S.Kawakami. *Electrochim. Acta*, **146**, 371 (2014)
107. H.Kondo, M.Matsumiya, K.Tsunashima, S.Kodama. *Electrochim. Acta*, **66**, 313 (2012)
108. H.Ota, M.Matsumiya, N.Sasaya, K.Nishihata, K.Tsunashima. *Electrochim. Acta*, **222**, 20 (2016)

109. N.Serizawa, S.Seki, K.Takei, H.Miyashiro, K.Yoshida, K.Ueno, N.Tachikawa, K.Dokko, Y.Katayama, M.Watanabe, T.Miura. *J. Electrochem. Soc.*, **160**, A1529 (2013)
110. M.Yamagata, N.Tachikawa, Y.Katayama, T.Miura. *Electrochemistry*, **73**, 564 (2005)
111. R.Fukui, Y.Katayama, T.Miura. *Electrochemistry*, **73**, 567 (2005)
112. Y.Katayama, R.Fukui, T.Miura. *J. Electrochem. Soc.*, **154**, D534 (2007)
113. K.Fujii, T.Nonaka, Y.Akimoto, Y.Umebayashi, S.-i.Ishiguro. *Anal. Sci.*, **24**, 1377 (2008)
114. A.-V.Mudring, A.Babai, S.Arenz, R.Giernoth. *Angew. Chem., Int. Ed.*, **44**, 5485 (2005)
115. N.Tachikawa, Y.Katayama, T.Miura. *Electrochemistry*, **77**, 642 (2009)
116. N.Tsuda, M.Matsumiya, K.Tsunashima, S.Kodama. *ECS Trans.*, **50**, 539 (2013)
117. V.A.Azov, K.S.Egorova, M.M.Seitkalieva, A.S.Kashin, V.P.Ananikov. *Chem. Soc. Rev.*, **47**, 1250 (2018)
118. T.Cui, A.Lahiri, T.Carstens, N.Borisenko, G.Pulletikurthi, C.Kuhl, F.Endres. *J. Phys. Chem. C*, **120**, 9341 (2016)
119. G.Feng, X.Jiang, R.Qiao, A.A.Kornyshev. *ACS Nano*, **8**, 11685 (2014)
120. A.V.Rudnev, K.Kiran, A.Cedeño López, A.Dutta, I.Gjuroski, J.Furrer, P.Broekmann. *Electrochim. Acta*, **306**, 245 (2019)
121. H.Kondo, M.Matsumiya, K.Tsunashima, S.Kodama. *ECS Trans.*, **50**, 529 (2013)
122. L.Sanchez-Cupido, J.M.Pringle, A.L.Siriwardana, A.Unzurrunzaga, M.Hilder, M.Forsyth, C.Pozo-Gonzalo. *J. Phys. Chem. Lett.*, **10**, 289 (2019)
123. R.Atkin, G.G.Warr. *J. Phys. Chem. C*, **111**, 5162 (2007)
124. R.Hayes, N.Borisenko, M.K.Tam, P.C.Howlett, F.Endres, R.Atkin. *J. Phys. Chem. C*, **115**, 6855 (2011)
125. Y.Fu, A.V.Rudnev. *Curr. Opin. Electrochem.*, **1**, 59 (2017)
126. S.Perkin, T.Albrecht, J.Klein. *Phys. Chem. Chem. Phys.*, **12**, 1243 (2010)
127. I.Bou-Malham, L.Bureau. *Soft Matter*, **6**, 4062 (2010)
128. N.V.Ignat'ev, P.Barthen, A.Kucheryna, H.Willner, P.Sartori. *Molecules*, **17**, 5319 (2012)
129. M.Galinski, A.Lewandowski, I.Stepniak. *Electrochim. Acta*, **51**, 5567 (2006)
130. L.M.Glukhov, A.A.Greish, L.M.Kustov. *Rus. J. Phys. Chem. A*, **84**, 104 (2010)
131. C.Jagadeeswara Rao, K.A.Venkatesan, K.Nagarajan, T.G.Srinivasan, P.R.Vasudeva Rao. *J. Nucl. Mater.*, **399**, 81 (2010)
132. E.Barrado, J.A.Rodríguez, Y.Castrillejo. *J. Electroanal. Chem.*, **804**, 148 (2017)
133. Q.B.Zhang, C.Yang, Y.X.Hua, Y.Li, P.Dong. *Phys. Chem. Chem. Phys.*, **17**, 4701 (2015)
134. A.Lewandowski, L.Waligora, M.Galinski. *Electroanal.*, **21**, 2221 (2009)
135. L.Asen, S.Martens, U. Heiz, A.C.Knoll, O. Schneider. *ECS Trans.*, **86**, 475 (2018)
136. S.Thomas, J.Mallet, H.Rinnert, M.Molinari. *RSC Adv.*, **8**, 3789 (2018)
137. C.A.Berger, M.Arkhipova, G.Maas, T.Jacob. *Nanoscale*, **8**, 13997 (2016)
138. J.Alvarez-Vicente, S.Dandil, D.Banerjee, H.Q.N.Gunaratne, S.Gray, S.Felton, G.Srinivasan, A.M.Kaczmarek, R.Van Deun, P.Nockemann. *J. Phys. Chem. B*, **120**, 5301 (2016)
139. Z.G.Shamaeva, N.G.Marina, Y.B.Monakov, S.R.Rafikov. *Bull. Acad. Sci. USSR, Div. Chem. Sci.*, **31**, 743 (1982)
140. Y.I.Murinov, Y.B.Monakov, Z.G.Shamaeva, N.G.Marina, V.S.Kolosnitsyn, Y.E.Nikitin, S.R.Rafikov. *Bull. Acad. Sci. USSR, Div. Chem. Sci.*, **26**, 2581 (1977)
141. S.S.Korovin, O.V.Galaktionova, E.N.Lebedeva, G.N.Voronskaya. *Zh. Neorg. Khim.*, **20**, 908 (1975)
142. S.S.Korovin, E.N.Lebedeva, O.V.Galaktionova, T.I.Kaledina, V.G.Lebedev. *Zh. Neorg. Khim.*, **22**, 1328 (1977)
143. P.Bagri, H.Luo, I.Popovs, B.P.Thapaliya, J.Dehaudt, S.Dai. *Electrochem. Commun.*, **96**, 88 (2018)
144. G.M.Krishna, A.Rout, K.A.Venkatesan. *J. Electroanal. Chem.*, **856**, 113671 (2020)
145. M.Matsumiya, Y.Kikuchi, T.Yamada, S.Kawakami. *Sep. Purif. Technol.*, **130**, 91 (2014)
146. S.Murakami, M.Matsumiya, T.Yamada, K.Tsunashima. *Solvent Extr. Ion Exch.*, **34**, 172 (2016)
147. F.-M.Lin, C.L.Hussey. *J. Electrochem. Soc.*, **140**, 3093 (1993)
148. X.Yang, L.He, S.Qin, G.-H.Tao, M.Huang, Y.Lv. *PLOS ONE*, **9**, e95832 (2014)
149. M.Matsumiya, S.Suda, K.Tsunashima, M.Sugiya, S.-y.Kishioka, H.Matsuura. *J. Electroanal. Chem.*, **622**, 129 (2008)
150. A.Liu, Z.Shi, R.G.Reddy. *Metall. Mater. Trans. B*, **51B**, 1162 (2020)
151. A.M.P.Sakita, R.Della Noce, C.S.Fugivara, A.V.Benedetti. *Phys. Chem. Chem. Phys.*, **18**, 25048 (2016)
152. Y.Chen, H.Wang, B.Li. *RSC Adv.*, **5**, 39620 (2015)
153. G.Panzeri, L.Magagnin. *ECS Trans.*, **75**, 31 (2016)
154. X.Li, Z.Li, M.Orefice, K.Binnemans. *ACS Sustain. Chem. Eng.*, **7**, 2578 (2019)
155. H.Sepehri-Amin, S.Hirosawa, K.Hono. In *Handbook of Magnetic Materials*. Vol. 27. (Ed E.Brück). (Elsevier, 2018). P. 269
156. O.S.Anilturk, A.R.Koymen. *J.Magn. Magn. Mater.*, **272 – 276**, 531 (2004)
157. M.Y.Gao, C.Yang, Q.B.Zhang, J.R.Zeng, X.T.Li, Y.X.Hua, C.Y.Xu, Y.Li. *J. Electrochem. Soc.*, **164**, D778 (2017)
158. F.Rosalbino, G.Borzone, E.Angelini, R.Raggio. *Electrochim. Acta*, **48**, 3939 (2003)
159. J.Durst, A.Rudnev, A.Dutta, Y.Fu, J.Herranz, V.Kaliginedi, A.Kuzume, A.A.Permyakova, Y.Paratcha, P.Broekmann, T.J.Schmidt. *Chimia*, **69**, 769 (2015)
160. D.Gao, Y.Zhang, Z.Zhou, F.Cai, X.Zhao, W.Huang, Y.Li, J.Zhu, P.Liu, F.Yang, G.Wang, X.Bao. *J. Am. Chem. Soc.*, **139**, 5652 (2017)
161. D.Esrafilzadeh, A.Zavabeti, R.Jalili, P.Atkin, J.Choi, B.J.Carey, R.Brkljača, A.P.O'Mullane, M.D.Dickey, D.L.Officer, D.R.MacFarlane, T.Daeneke, K.Kalantar-Zadeh. *Nat. Comm.*, **10**, 865 (2019)
162. K.Mech, J.Mech, P.Zabinski, R.Kowalik, M.Wojnicki. *J. Electroanal. Chem.*, **748**, 76 (2015)
163. O.Berkh, N.Eliaz, E.Gileadi. *J. Electrochem. Soc.*, **161**, D219 (2014)
164. L.Ma, X.Xi, Z.Nie, T.Dong, Y.Mao. *Int. J. Electrochem. Sci.*, **12**, 1034 (2017)
165. X.-f.Long, G.-h.Guo, X.-h.Li, Q.-l.Xia, J.-f.Zhang. *Thin Solid Films*, **548**, 259 (2013)
166. M.Schwartz, N.V.Myung, K.Nobe. *J. Electrochem. Soc.*, **151**, C468 (2004)
167. X.Wang, L.Han, Y.Zhang, S.Xue. *J. Nanopart. Res.*, **18**, 67 (2016)
168. J.Chen, L.Rissing. *J.Appl. Phys.*, **109**, 07A766 (2011)
169. J.C.Wei, M.Schwartz, K.Nobe. *ECS Trans.*, **1**, 273 (2006)
170. J.C.Wei, M.Schwartz, K.Nobe. *J. Electrochem. Soc.*, **155**, D660 (2008)
171. T.Akiyama, H.Fukushima. *ISIJ Int.*, **32**, 787 (1992)
172. N.Zech, E.J.Podlaha, D.Landolt. *J. Electrochem. Soc.*, **146**, 2892 (1999)
173. O.Younes-Metzler, L.Zhu, E.Gileadi. *Electrochim. Acta*, **48**, 2551 (2003)
174. X.Xu, S.Sturm, J.Zavasnik, K.Z.Rozman. *ChemElectroChem*, **6**, 2860 (2019)
175. E.B.Molodkina, M.R.Ehrenburg, P.Broekmann, A.V.Rudnev. *Electrochim. Acta*, **299**, 320 (2019)

176. M.Manjum, N.Serizawa, A.Ispas, A.Bund, Y.Katayama. *J. Electrochem. Soc.*, **167**, 042505 (2020)
177. A.Ispas, M.Buschbeck, S.Pitula, A.Mudring, M.Uhlemann, A.Bund, F.Endres. *ECS Trans.*, **16**, 119 (2009)
178. M.U. Ceblin, S.Zeller, B.Schick, L.A.Kibler, T.Jacob. *ChemElectroChem*, **6**, 141 (2019)
179. Q.Rayée, T.Doneux, C.Buess-Herman. *Electrochim. Acta*, **237**, 127 (2017)
180. P.Sebastian, M.I.Giannotti, E.Gómez, J.M.Feliu. *ACS Appl. Energy Mater.*, **1**, 1016 (2018)
181. A.P.Abbott, G.Capper, K.J.McKenzie, K.S.Ryder. *J. Electroanal. Chem.*, **599**, 288 (2007)
182. M.Landa-Castro, J.Aldana-González, M.G.Montes de Oca-Yemha, M.Romero-Romo, E.M.Arce-Estrada, M.Palomar-Pardavé. *J. Alloys Compd.*, **830**, 154650 (2020)
183. P.Liu, Y.-P.Du, Q.-Q.Yang, G.-R.Li, Y.-X.Tong. *Electrochim. Acta*, **52**, 710 (2006)
184. P.Liu, Y.Du, Q.Yang, Y.Tong, G.A.Hope. *J. Electrochem. Soc.*, **153**, C57 (2006)
185. S.-L.Wang, J.-B.Lin, Q.-Y.Cai, Y.Zhang. *J. Alloys Compd.*, **450**, 142 (2008)
186. J.Li, H.Lai, B.Fan, B.Zhuang, L.Guan, Z.Huang. *J. Alloys Compd.*, **477**, 547 (2009)
187. M.Li, B.Q.Chen, T.T.Xiong, L.X.Gao, C.Du, Y.N.Zhu, S.M.Zhang. *J. Dispersion Sci. Technol.*, **41**, 941 (2020)
188. E.Gómez, P.Cojocaru, L.Magagnin, E.Valles. *J. Electroanal. Chem.*, **658**, 18 (2011)
189. E.Gómez, E.Valles, P.Cojocaru, A.Raygani, L.Magagnin. *ECS Trans.*, **41**, 3 (2012)
190. P.Cojocaru, L.Magagnin, E.Gomez, E.Vallés. *Mater. Lett.*, **65**, 3597 (2011)
191. K.Kopczyński, G.Lota. *Electrochem. Commun.*, **107**, 106538 (2019)
192. G.Panzeri, M.Tresoldi, C.Rinaldi, L.Magagnin. *J. Electrochem. Soc.*, **164**, D930 (2017)
193. Y.Yang, C.Xu, Y.Hua, M.Wang, Z.Su. *Ionics*, **23**, 1703 (2017)
194. I.Billard, C.Gaillard. *Radiochim. Acta*, **97**, 355 (2009)
195. K.Binnemans. In *Comprehensive Inorganic Chemistry II*. (Second Edition). (Eds J.Reedijk, K.Poeppelmeier). (Amsterdam: Elsevier, 2013). P. 641
196. L.C.Branco, J.N.Rosa, J.J.Moura Ramos, C.A.M.Afonso. *Chem. – Eur. J.*, **8**, 3671 (2002)
197. L.Yu, H.Sun, J.He, D.Wang, X.Jin, X.Hu, G.Z.Chen. *Electrochem. Commun.*, **9**, 1374 (2007)
198. P.Nockemann, B.Thijs, T.N.Parac-Vogt, K.Van Hecke, L.Van Meervelt, B.Tinant, I.Hartenbach, T.Schleid, V.T.Ngan, M.T.Nguyen, K.Binnemans. *Inorg. Chem.*, **47**, 9987 (2008)
199. I.Krossing, I.Raabe. *Angew. Chem., Int. Ed.*, **43**, 2066 (2004)
200. C.Chiappe, M.Malvaldi, B.Melai, S.Fantini, U. Bardi, S.Caporali. *Green Chem.*, **12**, 77 (2010)
201. S.R.Batten, R.Robson, S.R.Batten, P.Jensen, B.Moubaraki, K.S.Murray. *Chem. Commun.*, 439 (1998)
202. A.Entezari-Zarandi, F.Larachi. *J.Rare Earths*, **37**, 528 (2019)
203. A.P.Abbott, G.Capper, D.L.Davies, K.J.McKenzie, S.U.Obi. *J. Chem. Eng. Data*, **51**, 1280 (2006)
204. W.Chen, J.Jiang, X.Lan, X.Zhao, H.Mou, T.Mu. *Green Chem.*, **21**, 4748 (2019)
205. P.Nockemann, B.Thijs, S.Pittois, J.Thoen, C.Glorieux, K.Van Hecke, L.Van Meervelt, B.Kirchner, K.Binnemans. *J. Phys. Chem. B*, **110**, 20978 (2006)
206. H.Li, D.Li, Y.Wang, Q.Ru. *Chem. – Asian J.*, **6**, 1443 (2011)
207. P.Nockemann, B.Thijs, N.Postelmans, K.Van Hecke, L.Van Meervelt, K.Binnemans. *J. Am. Chem. Soc.*, **128**, 13658 (2006)
208. T.Ohaion, Y.Kalisky, Y.Ben-Eliyahu, J.Y.Becker, A.Bettelheim. *Eur. J. Inorg. Chem.*, **2013**, 3477 (2013)
209. W.J.Oldham, D.A.Costa, W.H.Smith. In *Ionic Liquids*. Vol. 818. (ACS Symposium Series, 2002). P. 188
210. M.Yoshizawa, W.Xu, C.A.Angell. *J. Am. Chem. Soc.*, **125**, 15411 (2003)
211. M.Hayyan, F.S.Mjalli, M.A.Hashim, I.M.AlNashef, T.X.Mei. *J. Ind. Eng. Chem.*, **19**, 106 (2013)
212. A.V.Rudnev, K.Kiran, P.Broekmann. *ChemElectroChem*, **7**, 1897 (2020)
213. S.Lerch, T.Strassner. *Chem. – Eur. J.*, **25**, 16251 (2019)
214. E.P.Grishina, N.O.Kudryakova, L.M.Ramenskaya, Y.A.Fadeeva. *Rus. J. Phys. Chem. A*, **92**, 724 (2018)
215. R.Alcalde, M.Atilhan, S.Aparicio. *J. Mol. Liq.*, **258**, 1 (2018)
216. F.Yang, Q.Ma, X.Wang, Z.Liu. *J. Chem. Eng. Data*, **62**, 1628 (2017)
217. O.Ciocirlan, O.Croitoru, O.Iulian. *J. Chem. Thermodyn.*, **101**, 285 (2016)
218. V.V.Chaban, O.V.Prezhdo. *J. Phys. Chem. Lett.*, **2**, 2499 (2011)
219. D.V.Vasilyev, A.V.Rudnev, P.Broekmann, P.J.Dyson. *ChemSusChem*, **12**, 1635 (2019)